Design of Cathepsin K Inhibitors for Osteoporosis

David N. Deaton* and Francis X. Tavares*

Department of Medicinal Chemistry, GlaxoSmithKline, Research Triangle Park, North Carolina, 27709, USA

Abstract: Osteoporosis is a progressive, debilitating bone disease resulting in increased cost and morbidity to the elderly. This review summarizes the therapeutic approaches taken in the treatment of osteoporosis with particular emphasis on cathepsin K inhibitors. Cathepsin K, a cysteine protease predominantly expressed in osteoclasts, is a key player involved in bone matrix degradation. Both genetic ablation and small molecule inhibitor strategies versus cathepsin K have validated the importance of this enzyme in bone resorption. Starting from aldehyde-based leads, this review synopsizes the design of improved small molecule inhibitors by GlaxoWellcome researchers. These efforts involved the evaluation of various warheads, including cyanamides, ketoheterocycles, and ketoamides. Initial structure/activity relationships of aldehyde-based inhibitors proved useful in the design of ketoamide-based cathepsin K inhibitors. Further exploration of S^3, S^2, S^1, and $S^{1'}$ subsites with P^3, P^2, P^1, and $P^{1'}$ probes have resulted in the identification of potent, selective, orally bioavailable ketoamide-based inhibitors of cathepsin K with demonstrated *in vivo* efficacy.

INTRODUCTION

Osteoporosis is a debilitating disease increasingly found in the geriatric population [1,2]. With the increase in the population of this group, osteoporosis results in an enormous fiscal burden on public health care systems. Although traditionally thought to be a disease associated with postmenopausal women arising from an estrogen deficiency and resulting in enhanced osteoclast formation and systemic osteolysis, osteoporosis is becoming more prevalent in geriatric males. Osteoporosis leads to an increased incidence of fractures among the elderly. Key elements in the risk of fracture include load bearing capacity of the skeletal element and bone strength. Bone is a dynamic organ undergoing continuous remodeling involving resorption and formation. A shift in the dynamic equilibrium of bone remodeling towards resorption, versus formation, results in skeletal microarchitectural deterioration, bone fragility, and susceptibility to fractures.

Most of the current therapies have focused on attenuating bone resorption by osteoclasts; these include estrogen, selective estrogen receptor modulators (SERMs), bisphosphonates, calcitonin, and $\alpha_v\beta_3$ antagonists. Since these agents repress bone remodeling, they potentially can result in the formation of adynamic, weak bones that are resistant to microfracture repair. The sex steroid estrogen plays an important role in males, in addition to females, in the bone remodeling process. Lack of the estrogen receptor α (ER-α) in males results in high rates of bone turnover and skeletal osteopenia [3]. In addition, the use of aromatase inhibitors in males prevents the formation of estrogen resulting in an increase in bone resorption with the suppression of bone formation markers [4]. The beneficial effects of estrogen arise from the suppression of the production of the receptor activator of nuclear factor κB ligand (RANK-L) and an increase in the secretion of osteoprotegerin (OPG), the decoy receptor for RANK-L [5,6]. Moreover, estrogen also induces apoptosis of osteoclasts *via* production of transforming growth factor β (TGF-β) by osteoblastic cells [7]. Furthermore, estrogen attenuates osteocyte apoptosis [8]. Although estrogen has beneficial effects on the bone, adverse side effects such as cancer and cardiovascular events have resulted in the search for SERMs that target only bone. Tamoxifen, raloxifene, and the newer SERMs such as lasofoxifene and toremifene are agents that share the beneficial effects of estrogen on bone [9-13].

Bisphosphonates are widely used as effective anti-osteoporosis agents [14]. Both simple and nitrogen containing bisphosphonates cause osteoclast apoptosis. The simple bisphosphonates cause apoptosis *via* replacement of the pyrophosphate group in ATP by a non-hydrolyzable bisphosphonate group leading to permeation of the mitochondrial membrane, release of cytochrome c and activation of caspase-3 [15]. The nitrogen containing bisphosphonates utilize an alternative pathway, inhibiting farnesyl diphosphate (FPP) synthase in the mevalonate pathway resulting in the depletion of FPP and geranylgeranyl diphosphate (GGPP). These are isoprenoid lipids essential for farnesylation, and geranylgeranylation of small molecule GTPases that regulate survival of osteoclasts [16]. Interestingly, HMG-CoA reductase inhibitors also cause osteoclast apoptosis by effecting the mevalonate pathway, inhibiting the formation of mevalonate from HMG-CoA to decrease the formation of prenylated proteins [17,18]. On the other hand, another anti-resorptive therapy, calcitonin, decreases the attachment of osteoclasts to bone tissue *via* invagination of the brush border membrane attenuating bone remodeling [19,20]. Calcitonin therapy does not significantly increase bone mineral density (BMD) but slower remodeling allows osteoblasts to lay down stronger, higher quality bone [21-23].

Integrins such as $\alpha_v\beta_3$ and $\alpha_v\beta_5$ mediate osteoclast bone attachment by recognizing Arg-Gly-Asp (RGD) motifs on extracellular matrix proteins [24]. Upon attachment, the cytoplasmic region of the transmembrane protein conveys secondary messengers that help in the formation of a well

*Address correspondence to DND or FXT at Department of Medicinal Chemistry, GlaxoSmithKline, Research Triangle Park, North Carolina, 27709, USA; DND: Tel.: 1-919-483-6270; E-mail: david.n.deaton @gsk.com; FXT: Tel: 1-919-483-7456; E-mail: francis.x.tavares@gsk.com

1568-0266/05 $50.00+.00

defined ruffled membrane for a resorptive microenvironment involving cytoskeletal reorganization. Deletion of $\alpha_v\beta_3$ integrin results in osteoclast dysfunction resulting in osteosclerosis [25], while $\alpha_v\beta_5$ (-/-) mice exhibit enhanced osteoclasto-genesis and increased bone resorption [26]. Small molecule RGD mimetics bind to $\alpha_v\beta_3$ integrins, inhibiting osteoclast bone recognition and reducing bone resorption [27,28]. Phase II studies in humans using MRL123 have validated $\alpha_v\beta_3$ integrin antagonism as a viable strategy to block osteoclast attachment, disrupt signalling, and decrease bone resorption [29]. Since most $\alpha_v\beta_3$ integrin antagonists lack selectivity versus $\alpha_v\beta_5$, enhanced specificity for $\alpha_v\beta_3$ could lead to increased anti-resorptive efficacy.

Mechanisms, such as blockage of the ClC-7 chloride channel [30,31] or the bicarbonate/chloride exchanger or inhibition of the osteoclastic V-type H^+-ATPase [32-34] or carbonic anhydrase II [35-37], that impair acidification of the absorption lacunae during the resorption process, result in decreased bone resorption and unaltered bone formation. The decrease in pH is mediated by active transport of protons over the ruffled border membrane by an osteoclastic vacuolar H^+-ATPase, the membrane potential generated by this process is dissipated by the passage of Cl^- ions through ClC-7 chloride channels. In addition, the osteoclast maintains a continuous supply of cytosolic H^+ and HCO_3^- by the action of carbonic anhydrase II (CA-II) [38]. Normal intracellular pH is also maintained by the bicarbonate/ chloride exchanger [39]. Another approach to inhibit acidification during the resorption process is to block the Na^+/H^+ antiporter [40]. Any of these strategies to inhibit acidification of the resorption lacunae are attractive, but considerations regarding tissue selectivity for these targets need to be addressed [41,42]. H^+-ATPase inhibitors with moderate osteoclast selectivity demonstrate the feasibility of resorption impairment *via* this mechanism [43,44].

Recently anabolic bone agents have been pursued as useful anti-osteoporotic agents. Although sustained elevation of parathyroid hormone (PTH) causes bone erosion, pulsatile administration results in net bone formation *via* increased bone remodeling coupled with attenuated osteoblast apoptosis. This realization has resulted in the development of a recombinant form of this anabolic bone stimulant called teriparatide (rhPTH (1-34)) [45,46]. Its high cost, subcutaneous route of administration, and osteosarcoma risk limit its usefulness. Since the parathyroid gland specific calcium-sensing receptor modulates PTH secretion, antagonism of this 7-TM protein to stimulate endogenous production of PTH induces bone turnover [47,48]. Orally bioavailable antagonists of this receptor could address some of the limitations of recombinant PTH.

Androgen depletion results in a decrease in bone mass and osteoporosis. Androgens suppress RANK-L induced osteoclast differentiation and also are directly involved in inhibiting the activity of mature osteoclasts [49,50]. The development of selective, tissue specific androgen receptor modulators, that can prevent prostrate hyperplasia or cancer and have the desirable osteoanabolic activities of 5α-dihydrotestosterone (DHT), is an area of increasing research. Considerable advances have been realized in this endeavor [51-54]. Furthermore, strategies to stimulate bone morphogenic proteins (BMPs) to initiate new bone formation are also an area of intense research. Sclerostin competes with BMPs for type I and type II BMP receptor binding, resulting in attenuation of BMP signaling and suppression of osteoblast activity and subsequent bone formation [55,56]. A monoclonal antibody to sclerostin increases BMD [57]. Alternatively, BMP-2 modulators such as the widely used HMG-CoA reductase inhibitors as well as 20S proteasome inhibitors stimulate bone formation [58], although lower fracture risk was not noted in patients treated with HMG-CoA reductase inhibitors. Moreover, the anabolic agent strontium ranelate inhibits bone resorption and stimulates bone formation [59,60]. Strontium ranelate has been shown to reduced vertebral and non-vertebral fractures in postmenopausal women [61,62].

Recently cell to cell adhesion machinery has been found to be important in bone morphology [63]. Cadherins on the surface of one cell can homodimerize with those on a proximal one to form Ca^{2+}-dependent adherens junctions. Such cross talk interactions are important for osteoblast differentiation. For example, disruption of cadherin signaling using antibodies, antisense RNA, or overexpression of a dominant negative cadherin transcript impairs osteoclast differentiation [64-66]. In addition, cell to cell interactions, involving gap junctions composed of an array of connexin molecules, form a transcellular junction between osteoblasts and osteocytes, propagating calcium waves among coupled cells. These interactions are necessary for development and maintenance of a differentiated osteoblast phenotype [67-69].

Several factors control the differentiation of monocyte-family precursors to mature osteoclasts. The essential role of RANK-L or its receptor, RANK, in osteoclastogenesis is underscored by the fact that mice lacking RANK-L or RANK are devoid of osteoclasts [70,71]. Furthermore, RANK-L monoclonal antibodies have shown anti-resorptive benefits in the clinic [72,73]. Membrane bound macrophage colony stimulating factor (M-CSF) is also a critical modulator of osteoclast formation, as M-CSF treatment directly induces RANK expression [74]. Low molecular weight hyaluronic acid (LMWHA), a component of the extracellular matrix has been shown to enhance osteoclast formation *via* interaction of RANK and RANK-L [75]. Factors independent of RANK/RANK-L signaling are also important players in this arena. For example, mice deficient in PU.1, a transcription factor which is essential for early macrophage maturation, become osteopetrotic [76]. Moreover, the differentiation of macrophages to osteoclast is controlled by a plethora of cytokines including IL-1, IL-3, IL-4, IL-6, IL-10, IL-13, IL-14, GM-CSF, MS-CSF, and TNFα. Of these, IL-4, IL-10, IL-13, and IL-14 are known to inhibit osteoclast formation [77-83]. In addition, the osteoblast secreted RANK-L decoy receptor OPG is a strong inhibitor of osteoclast formation [84-86]. Overexpression of OPG in transgenic mice results in osteopetrosis, whereas OPG deficient mice have an osteoporotic phenotype [87]. As RANK-L and OPG have opposing effects, the ratio of RANK-L to OPG governs osteogenesis. The RANK-L:OPG is also controlled by TGF-β, which stimulates OPG formation and suppresses RANK-L expression [88,89]. Tartrate-resistant acid phosphatase (TRAP/Acp5), activated

by proteolytic cleavage with cathepsin K or cathepsin L, is highly expressed in osteoclasts [90-92]. Mice deficient in TRAP are mildly osteopetrotic [93]. In addition, these mice have altered ruffled borders and disturbed intracellular vesicular transport [94]. In contrast, mice overexpressing TRAP display an osteoporotic phenotype [95].

Transcription factors such as activator protein 1 (AP-1) and NF-κB, both down stream effectors of RANK-L, have been increasingly recognized as potential targets for inhibition of resorption, since they promote osteoclast formation. Furthermore, kinase inhibitors of c-Jun N-terminal kinase (JNK) and IκB kinase β (IKKβ), that down regulate AP-1 and NF-κB, respectively, might be useful approaches to modulate osteoclast activity [96,97]. NF-κB essential modifier (NEMO) is a regulatory component that associates with the C terminus of the catalytic subunits of both the α- and β-IκB kinase complex called the NEMO-binding domain (NBD). Disruption of the association of the NEMO with the IκB subunits *via* a NBD peptide results in inhibition of osteoclastogenesis and inflammatory bone destruction [98]. Likewise, the high osteoclastic expression of Src tyrosine kinase coupled with the osteopetrotic phenotype of c-Src (-/-) mice have made this kinase an attractive osteoporosis target [99-103]. In addition, the increased osteoblast numbers and bone formation rates in Src (-/-) mice indicate that Src tyrosine kinase affects both bone deposition and bone removal [104]. The effects of Src inhibition on the bone resorption process are attributed to the lack of formation of the osteoclastic ruffled border in Src (-/-) mice as well as a decrease in osteoclast motility [105-107]. Finally, serine threonine kinase inhibitors, such as GSK-3 inhibitors, that affect wnt signalling, also increase bone formation *in vitro* and *in vivo* [108].

Bone is a complex organ composed of inorganic mineral, hydroxyapatite ($Ca_{10}(PO_4)_6(OH)_2$), and an organic matrix mainly composed of Type I collagen. Dissolution of the inorganic phase precedes degradation of the type I collagen matrix. Several steps are orchestrated before bone resorption takes place. Osteoclasts, derived from haematopoietic precursors, utilize integrin proteins to bind bone matrix proteins containing Arg-Gly-Asp (RGD) motifs to form an enclosed environment known as the resorption lacunae. The formation of this ruffled bordered sealed zone results in polarization of the membrane into basolateral and apical membranes allowing for dissolution of the inorganic phase *via* acidification of the extracellular space. The vacuolar H^+-ATPase, a proton pump embedded in the ruffled border of the basolateral membrane, secretes the acid with charge neutrality maintained by the ClC-7 chloride channel. The H^+-ATPase not only leads to the dissolution of hydroxyapatite, but the lowered pH of the resorption lacunae, results in the activation of the secreted lysosomal cysteine protease cathepsin K, a potent collagenase that is unique in its ability to cleave the triple helical and telopeptide regions of Type I collagen [109]. The specificity of cathepsin K for collagen *vs* gelatin and other substrates depends on the tertiary nature of the protein, wherein a 1:1 association of five cathepsin K and chondroitin molecules is necessary for collagenase activity. Monomeric cathepsin K can cleave non-Type I collagen substrates [110]. Solubilization of the inorganic mineral by the acidic solution necessarily precedes exposure of the organic matrix to degradation by cathepsin K. Acid activation of cathepsin K involves autocatalytic cleavage of the proenzyme resulting in dissociation of the 99-amino acid propeptide region of the protein which normally binds the active site and blocks its enzymatic activity [111,112]. The identification of serum carboxyterminal telopeptide of type I collagen (CTX) as a cleavage product resulting from the actions of cathepsin K has led to its proven usefulness as a bone resorption marker in clinical trials [113]. Interestingly, cathepsin K has differential effects on bone resorption on cortical *vs* trabecular bone. In transgenic mice over-expressing cathepsin K, there is an increase in osteopenia of metaphyseal trabecular bone and an increase in porosity of diaphyseal cortical bone. Further, in addition to increased porosity of the diaphyseal cortical bone, there was an increase in its thickness and mineral density [114]. Cathepsin K is a cysteine protease of the CA C1 family, represented by papain, containing a conserved catalytic triad of ^{25}Cys, ^{162}His, and ^{182}Asn and is abundantly and selectively expressed in osteoclasts. The high expression of this enzyme in osteoclasts suggests its crucial nature for bone resorption [115-118]. Mutations in human cathepsin K leading to pycnodysostosis, a rare osteopetrotic disease characterized by abnormal bone resorption, have been demonstrated [119-122]. Moreover, cathepsin K deficient mice exhibit a distinct osteopetrotic phenotype [123,124]. Contrary to historical suppositions, cathepsin K, and not cathepsin L, is the major protease responsible for human osteoclastic bone resorption [125]. Cathepsin K antisense nucleotides inhibit osteoclast mediated bone resorption [126]. Furthermore, glycos-aminoglycans (GAGs) are known to form cathepsin K-GAG complexes that enhance collagenase activity of cathepsin K in osteoclast while inhibiting its elastolytic activity [127]. In addition, cathepsin K overexpression results in high bone turnover in mice [128]. The importance of cathepsin K, and not cathepsins B, L and S, towards bone resorption has been demonstrated using small molecule peptidyl vinyl sulfones [129,130]. Besides its expression in osteoclasts, cathepsin K is also expressed in monocyte-derived macrophages [131], adipocytes [132], thyroid epithelial cells [133], bronchial epithelial cells [134], ovarian theca cells [135], activated stellate cells [136], Sertoli cells [137], gastric parietal cells [138], and synovial fibroblasts [139] as well as several disease states including rheumatoid arthritis [140], metastatic prostate cancer [141] and lung tumors [142], lung fibrosis [134], atherosclerosis [143], and osteoarthritis [144]. As opposed to osteoclast organic matrix, 90% of which is composed of type I collagen, cartilage tissue is mainly composed of type II collagen and aggrecan. Cathepsin K efficiently degrades both type II collagen and aggrecan in cartilage tissue, such proteolysis is often observed in rheumatoid arthritis [145-147]. Results from genetic studies eliminating cathepsin K have been validated using small molecule inhibitors. The irreversible nonselective cysteine protease inhibitor E-64 attenuates osteoclastic bone resorption [148,149]. Furthermore, cathepsin K specific inhibitors, such as cyclic ketones [150,151], ketoamides [152,153], and dipeptidyl nitriles [154], exhibit *in vivo* activity when administered orally to either rodents or primates. Finally, several pharmaceutical companies are currently performing clinical trials, with Novartis having

reported reductions in bone resorption markers in humans with one selective cathepsin K inhibitor [155,156].

Due to a large number of cysteine proteases identified in the human genome, selectivity of inhibitors of cathepsin K versus other cysteine proteases, especially those that are highly homologous such as cathepsins L (60% identity, 76% similarity), S (59% identity, 73% similarity) and V (58% identity, 62% similarity), is always a major concern [157,158]. Cysteine proteases such as cathepsin S and L are expressed in the lysosomal compartments of antigen presenting cells such as dendritic cells, B-cells and macrophages and are involved in processing of antigenic peptides and also cleavage of the invariant chain that blocks the antigen-binding site of the MHC class II molecule. Although the former process is mostly redundant since several cathepsins usually are capable of degrading the same antigenic peptide, the latter process, i.e. invariant chain processing, depends on the presence of a particular cysteine protease [159-161]. The antigenic peptide fragments that are bound to the major histocompatibility complex (MHC) class II are transported to the surface of antigen presenting cells for recognition by $CD4^+$ T cells [162]. Such antigen processing is crucial for the body's response to pathogens but is also sometimes responsible for adverse effects such as allergies and autoimmune disease. Endothelial progenitor cells expressing cathepsin L have been found to be extremely important in neovascularization, an adaptation process to rescue tissue from critical ischemia. Mice lacking cathepsin L show impaired functional recovery following hind limb ischemia [163]. Cathepsin V is expressed in the thymus and testis and is also involved in MHC class II antigen presentation. In addition, cathepsin V along with cathepsins K and S have potent elastolytic activity resulting in destruction of elastin matrix in atherosclerotic arteries [164]. In the design of selective cathepsin K inhibitors, there are several key elements that need to be addressed. These inhibitors need to be reversible so as to prevent antigenicity arising from covalent modification of proteins *via* irreversible inhibition. Selectivity over other cysteine and serine proteases is also desirable to prevent adverse side effects. Most of the cathepsin K inhibitors reported take advantage of the differences in the S^2 subsite to gain selectivity for cathepsin K versus other cysteine proteases. The differential requirements of the S^2 subsite, i.e. the larger S^2 pockets for cathepsins S and L versus the shallower S^2 pocket of cathepsin K, in combination with differences in S^3 subsites can afford selective cathepsin K inhibitors [129,165,150]. Selectivity gains using the S^1 prime subsite have also been reported for the ketoamide class of inhibitors [152,153]. Finally, in the design of cathepsin K inhibitors, sequence identity/homology among species needs to be considered so that a suitable pharmacodynamic model can be utilized to assist translation to the clinic. For example, in the design of cathepsin K inhibitors, variations in the S^2 and S^3 subsites can affect potency of inhibitors in the human *vs* rat orthologs resulting in considerable loss in potency at the rat enzyme.

ALDEHYDES

Knowing that cysteine protease inhibitors like leupeptin and E-64 attenuated bone resorption, Larry Miller, an osteoporosis expert in GlaxoWellcome's pharmacology department, was particularly excited about the discovery of cathepsin OC-2 in rabbit osteoclasts [115] and the subsequent identification of the human ortholog, cathepsin K [116,166,117,167,168]. When additional target validation was disclosed from Bruce Gelb's laboratory showing that the osteopetrotic disorder pycnodysostosis was caused by inactivating mutations in cathepsin K [120], Larry initiated a cathepsin K inhibitor program for the treatment of osteoporosis in 1996. As part of that program, a directed screen of known cysteine and serine protease inhibitors in the GlaxoWellcome compound collection was pursued. This screen identified calpeptin **1**, Cbz-Leu-Nle-H, as a very potent cathepsin K inhibitor (IC_{50} = 0.11 nM) [169]. Further focussed screening of close calpeptin analogs revealed that the single amino acid derivative Boc-Nle-H **2** was also a potent cathepsin K inhibitor (IC_{50} = 51 nM). Although ~500-fold less potent than calpeptin, this truncated inhibitor's absence of amide bonds and small size suggested it was an excellent lead molecule for further optimization.

In addition to synthesizing heavy atom derivatives of calpeptin to aid in phasing of potential x-ray diffraction patterns of cathepsin K/inhibitor co-crystals, synthesis of P^1 modified aldehydes was instituted to probe the S^1 subsite of cathepsin K [169]. The inhibitors were synthesized from the corresponding *tert*-butyloxycarbonyl-protected amino acids *via* mixed anhydride reduction, followed by oxidation. As shown in Table **1**, the glycine derivative **3** (IC_{50} = 5,800 nM) was ~100-fold less active than the starting lead, while the alanine derivative **4** (IC_{50} = 200 nM) was only ~4-fold less potent. Longer *n*-alkyl chains **5**, **8**, **18**, and **19** were equipotent to the Boc-Nle-H lead. In addition to enhancements in inhibitory potency from hydrophobic interactions of the aliphatic chain with the enzyme, the conformational bias induced by the side chain substituent may also contribute to the enhanced activity of the alanine derivative compared to the glycine analog.

Branching at the α-carbon of the P^1 moiety was detrimental to activity with the *tert*-butyl analog **7** (IC_{50} = 52,000 nM) being ~1,000-fold less active that the starting lead. Substitution at the β-carbon of the P^1 group was better tolerated with the leucine derivative **12** (IC_{50} = 31 nM) being equipotent to **2**, and the neopentyl analog **13** (IC_{50} = 250 nM) only suffering a slight decrease in activity. Unsaturation in the alkyl chain was also explored. The Z-alkene **15** (IC_{50} = 41 nM) was equivalent to **2**, whereas the E-alkene **16** (IC_{50} = 150 nM) and alkyne **17** (IC_{50} = 410 nM) suffered decreases in activity, possibly revealing information about the conformation of the P^1 alkyl chain.

Probing for potential π-π stacking interactions, aryl rings were tethered to the P^1 position. These analogs maintained good activity with the phenpropyl analog **30** (IC_{50} = 15 nM) being slightly more potent than **2**. The cyclohexyl derivatives were also active. The modest gains in activity suggest no π-π stacking interactions were achieved. Furthermore, the improvements were less attractive considering their synthetic complexity and decreased hydrophilicity.

Heteroatoms were also incorporated into the P^1 groups to probe the electronics of the S^1 subsite. Replacements of the β- or γ-carbon with "hard" heteroatoms like oxygen **20** or **22**

Table 1. Aldehyde P[1] Cathepsin K Inhibition

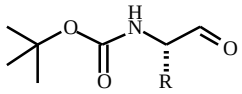

#	R	IC_{50} nM
3	H	5800
4	Me	200
5	Et	58
6	*i*-Pr	160
7	*t*-Bu	52,000
8	*n*-Pr	38
9	CH(Me)Et (S)	250
10	CH(Me)Et (R)	130
11	$CH_2C(CH3)=CH2$	79
12	CH_2*i*-Pr	31
13	CH_2*t*-Bu	250
2	*n*-Bu	51
14	$(CH_2)_3CF_3$	87
15	Z $CH_2CH=CHCH_3$	41
16	E $CH_2CH=CHCH_3$	150
17	$CH_2C{\equiv}CCH_3$	410
18	*n*-Pentyl	110
19	*n*-Hexyl	23
20	CH_2OEt	660
21	CH_2SEt	83
22	$(CH_2)_2OMe$	680
23	$(CH_2)_2SMe$	78
24	Ph	51
25	Cy	26
26	CH_2Ph	110
27	CH_2Cy	36
28	$(CH_2)_2Ph$	30
29	$(CH_2)_2Cy$	26
30	$(CH_2)_3Ph$	15
31	$(CH_2)_3Cy$	16
32	CH_2OCH_2Ph	38
33	CH_2SCH_2Ph	40
34	CH_2NHCO_2Me	370

(Table 1) Contd….

#	R	IC_{50} nM
35	$(CH_2)_4NHCO_2Me$	15
36	$(CH_2)_2N(Me)COCF_3$	98
37	$(CH_2)_3N(Me)COCF_3$	29
38	$(CH_2)_4N(H)COCF_3$	41
39	$(CH_2)_4N(Me)COCF_3$	50

or nitrogen **34** was detrimental to inhibitory activity. In contrast, the correspondingly "soft" sulfur analogs **21** and **23**, with d orbital occupation leading to more diffuse electron lone pairs, more closely resemble the carbon analogs and exhibit equal potency. Hard heteroatoms further removed from the amino acid backbone are well tolerated with the lysine-derived methylcarbamate **35** being quite potent (IC_{50} = 15 nM). The lysine and ornithine derived analogs should have enhanced aqueous solubility, potentially leading to better oral absorption.

With exploration of the S^1 subsite complete, the P^1 substituent was fixed as *n*-butyl and the S^2/ S^3 subsites were explored by modifications to the *tert*-butyl carbamate [170]. The carbamates were synthesized *via* coupling alcohols to the isocyanate derived from norleucine methyl ester. The esters were subsequently converted to the desired aldehydes. Alternatively, the alcohols were converted to chloroformates and coupled to the norleucine-derived aminoalcohol, then oxidized to the desired aldehydes. Since, the lead contained no P^3 moiety, an aryl ring was appended to the carbamate by varying tether lengths hoping to pick-up binding from van der Waals interactions with the enzyme or π-π stacking interactions with potential aryl groups in S^2, S^3, or the active site trough. As shown in Table **2**, these aryl analogs **40**, **41**, and **42** were less active than the *tert*-butyl group, but the apparently more potent phenethyl P^3 substituent (IC_{50} = 270 nM) was combined with the *tert*-butyl P^2 moiety (IC_{50} = 51 nM), giving a net 4-fold improvement in potency for analog **43** (IC_{50} = 12 nM). To further probe the size of the S^2 pocket, the diethyl **45**, cyclobutyl **44**, cyclopentyl **46**, and cyclohexyl **47** analogs were prepared, with the cyclopentyl derivative **46** (IC_{50} = 0.35 nM) being optimal.

To ascertain the importance to enzyme binding of both methyl substituents in analog **43**, the monomethyl diastereomers were prepared. All of the activity resided in the (S)-methyl diastereomer **48** (IC_{50} = 1.8 nM), which was more potent that the starting *gem* dimethyl analog **43**. In contrast, the (R)-methyl diastereomer was deleterious to enzyme activity. Having established the stereospecific inhibitory nature of these analogs, the active diastereomeric series was furthered explored, with the ethyl **51** (IC_{50} = 0.13 nM) and *iso*-propyl **53** (IC_{50} = 0.50 nM) derivatives being optimal.

To ease synthetic complexity, symmetrical P^2 substituents lacking a P^3 moiety were also investigated. The di-*iso*-propyl analog **58** (IC_{50} = 0.56 nM) was equipotent to the *iso*-propyl derivative **53**. In these symmetrical analogs **55-60**, one substituent likely occupies the S^2 pocket, while the other appendage may interact with the active site trough that normally accommodates the peptide backbone of substrates.

Several modifications to the aryl P^3 ring of analog **43** were explored. The cyclohexyl **50** and 3-thiophenyl **65** groups were similar to the phenyl ring. Furthermore, substitutions **61**-**64** to alter the electronic properties of the P^3 substituent had no effect on potency, suggesting modest interactions of the P^3 group with the enzyme.

Besides exploring the S^1, S^2, and S^3 subsites of the enzyme, the peptide backbone recognition motifs of cathepsin K were investigated by modifications to the core chain of analog **2** [171]. Probing the stereochemical requirements of cathepsin K substrates/inhibitors, the enantiomer of inhibitor **2** was prepared. The enantiomer of inhibitor **2** was a substantially poorer inhibitor of cathepsin K (IC_{50} = 5,900 nM). Since its residual activity might reflect activity from small quantities of **2** generated by epimerization under the acidic conditions of the enzyme assay, further effort was made to test the potential of the protease to accommodate a D-amino acid derivative. The α-methyl derivative **66** was prepared. As shown in Table **3**, it was inactive at concentrations up to 13,000 nM, implying that the activity of the enantiomer of **2** probably arose from contamination with ~1% of **2**.

Many proteases bind the amide bonds of their substrates with hydrogen bonding recognition motifs. Continuing efforts to probe the peptide backbone recognition of the enzyme, the hydrogen bond donor NH of the carbamate was N-methylated to test this possibility. This analog **69** (IC_{50} = 12,000 nM) was ~200 times less potent than **2**. This suggests that the proton is crucial for formation of a key hydrogen bond, although the protease may be unable to accommodate the methyl group in this region of the enzyme. To further investigate this potential hydrogen bonding interaction, the NH of the carbamate was replaced with oxygen **67** (IC_{50} = 1,900 nM) resulting in a ~37-fold decrease in inhibitory activity, providing further support for a potential hydrogen bond interaction with cathepsin K. Moreover, the methylene replacement **68** (IC_{50} = 3,500 nM) was also substantially less active, providing additional evidence for the hypothesis.

To further explore the requirements of the main chain of the inhibitor class, the importance of the carbamate oxygen was also investigated. The sulfur replacement provided the thiocarbamate **72** (IC_{50} = 2.2 nM) which was equipotent to

Table 2. Aldehyde P^2 - P^3 cathepsin K inhibition

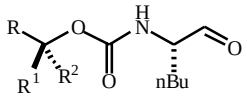

#	R	R^1	R^2	IC_{50} nM
2	Me	Me	Me	51
40	Ph	H	H	540
41	$PhCH_2$	H	H	270
42	$Ph(CH_2)_2$	H	H	600
43	$PhCH_2$	Me	Me	12
44	$PhCH_2$	$(CH_2)_3$		2.4
45	$PhCH_2$	Et	Et	2.1
46	$PhCH_2$	$(CH_2)_4$		0.35
47	$PhCH_2$	$(CH_2)_5$		2.0
48	$PhCH_2$	Me	H	1.8
49	$PhCH_2$	H	Me	100
50	$C_6H_{11}CH_2$	Me	H	2.7
51	$PhCH_2$	Et	H	0.13
52	$PhCH_2$	*n*Pr	H	1.5
53	$PhCH_2$	*i*Pr	H	0.50
54	$PhCH_2$	*i*Bu	H	6.5
55	$PhCH_2$	$PhCH_2$	H	71
56	H	Et	Et	4.0
57	H	*n*Pr	*n*Pr	0.87
58	H	*i*Pr	*i*Pr	0.56
59	H	*i*Bu	*i*Bu	1.1
60	Me	*i*Pr	*i*Pr	4.7
61	3-MeO-Ph CH_2	Me	Me	5.4
62	4-MeO-Ph CH_2	Me	Me	2.9
63	2-Cl-Ph CH_2	Me	Me	3.1
64	4-Cl-Ph CH_2	Me	Me	4.6
65	3-thiophenyl CH_2	Me	Me	7.6

the carbamate **71** (IC_{50} = 1.8 nM). In contrast, substitution of the oxygen with a methylene as in amide **70** (IC_{50} = 930 nM) resulted in a ~18-fold reduction in potency relative to the carbamate **2**. Attempts to replace the oxygen with NH were thwarted by its intramolecular cyclization onto the aldehyde warhead during oxidation of the alcohol. Blocking the nitrogen with a methyl substituent allowed the synthesis of urea **73** (IC_{50} = 3,300 nM), but it was ~1,800-fold less potent than the carbamate. The N-methyl of the urea may clash sterically with the surface of the active site of cathepsin K reducing its inhibitory potential.

Since selectivity is an important concern when designing potential drugs to avoid undesired toxicities, several of these aldehyde-based inhibitors were assayed versus the commercially available CA1 family cathepsins B & L [170]. As shown in Table **4**, all of these inhibitors were better inhibitors of cathepsin K than cathepsins B or L.

Table 3. Aldehyde Peptide Backbone Analog Cathepsin K Inhibition

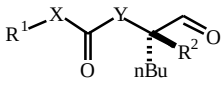

#	R^1	X	Y	R^2	IC_{50} nM
2	*t*-Bu	O	NH	H	51
66	*t*-Bu	O	NH	Me	>13,000
67	*t*-Bu	O	O	H	1,900
68	*t*-Bu	O	CH_2	H	3,500
69	*t*-Bu	O	NMe	H	12,000
70	*t*-Bu	CH_2	NH	H	930
71	(S)-$PhCH_2CHMe$	O	NH	H	1.8
72	(S)-$PhCH_2CHMe$	S	NH	H	2.2
73	(S)-$PhCH_2CHMe$	NMe	NH	H	3,300

Table 4. Aldehyde Cathepsin B, K, and L Inhibition and Selectivity

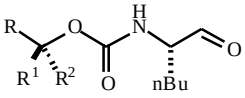

#	R	R^1	R^2	Cat B IC_{50} nM	Cat K IC_{50} nM	Cat L IC_{50} nM
44	$PhCH_2$	$(CH_2)_3$		3,400	2.4	1,200
45	$PhCH_2$	Et	Et	2,200	2.1	110
46	$PhCH_2$	$(CH_2)_4$		810	0.35	2,000
47	$PhCH_2$	$(CH_2)_5$		12,000	2.0	8,500
48	$PhCH_2$	Me	H	460	1.8	740
50	$C_6H_{11}CH_2$	Me	H	400	2.7	270
51	$PhCH_2$	Et	H	72	0.13	15

Furthermore, the cycloalkyl inhibitors **44**, **46**, and **47** were at least 500-fold more potent cathepsin K inhibitors than cathepsin B or L inhibitors. These results gave encouragement that selective cathepsin K inhibitors could be developed.

As shown in Figure (**1A**), Lisa Shewchuk solved an internal X-ray structure of cathepsin K co-crystallized with a *para*-bromo-derivative of calpeptin in 1997, the same year Axys [165] and SmithKline Beecham [172] disclosed their initial cathepsin K structures. This structure further validated conclusions drawn from the SAR. The presumed P^2 *iso*-butyl substituent did indeed occupy the S^2 pocket with the P^1 *n*-butyl moiety forming van der Waals interactions with the S^1 wall, and the P^3 phenyl group interacting with the S^3 groove. As expected based on papain x-ray structures with aldehydes, the hydroxyl of the hemithioacetal formed by addition of the active site thiol to the carbonyl occupies the oxy-anion hole where it is stabilized by hydrogen bonds to the backbone amide of ^{25}Cys, the side chain of ^{19}Gln, and the side chain of ^{162}His. Furthermore, there were two hydrogen bonds formed between the peptide recognition motif of the enzyme and the inhibitor confirming the backbone SAR data. The amide NH formed a hydrogen bond to the backbone carbonyl of ^{161}Asn, while its carbonyl oxygen accepted a hydrogen bond from the backbone NH of ^{66}Gly.

As expected based on their reputation, these aldehydes were rapidly metabolized during rat S9 liver incubations and

not detected after 15 minutes when dosed to male Han Wistar rat iv or po [170]. Despite these limitations, these efforts provided valuable structure/activity relationship information that it was hoped could be applied to the design of other cathepsin K inhibitors with different warheads.

SEMICARBAZONES

Since semicarbazones had been previously described as cysteine protease inhibitors [173], it was decided to explore this class of inhibitor. It was surmised that semicarbazones could provide access to $S^{1'}$ and $S^{2'}$ subsite binding interactions as well as potentially improve drug properties like aqueous solubility versus aldehydes. Numerous semicarbazones, derived from Boc-Nle-H **2**, were synthesized [174]. As shown in Table **5**, most of the terminally monosubstituted semicarbazones (**74**-**81**) were slightly less active than the starting aldehyde **2** with IC_{50}s ranging from 160-490 nM. Proximal substitution of a distally monosubstituted semicarbazone, as in analog **82**, substantially decreased potency relative to phenylethyl derivative **81**. In contrast, the terminally disubstituted semicarbazones (**83**-**89**) (IC_{50} = 35-72 nM) exhibited similar cathepsin K inhibitory activity to the starting aldehyde **2**.

The semicarbazones were generally stable in plasma with good membrane permeabilities. Furthermore, they had improved solubility in fasted state-simulated intestinal fluid (FS-SIF) relative to the parent aldehyde. Unfortunately, they were rapidly hydrolyzed to the starting aldehyde in simulated gastric fluid (SGF) as well as rapidly metabolized during rat S9 liver incubations. This *in vitro* instability translated to *in vivo* studies as these inhibitors had short terminal half-lifes, moderate to high clearances, moderate steady state volumes of distribution, and poor oral bioavailabilities in male Han Wistar rats. Like many different warhead inhibitor classes of cathepsin K inhibitors, the semicarbazones were substantially less potent inhibitors of the rat enzymes compared to the human ortholog. Despite these liabilities, several of these semicarbazones were able to attenuate bone resorption in an *ex vivo* rat calvaria resorption assay.

Many of these inhibitors were incubated with cathepsin K with the hope of obtaining co-crystals of sufficient diffraction quality for structural elucidation. Thirteen such crystals were identified, but structure refinement revealed aldehyde inhibitors with little or no electron density for the $P^{1'}$-$P^{2'}$ semicarbazide-derived portion of the inhibitor. For example as shown in Figure (**1B**), a co-crystal structure of a semicarbazone derivative of aldehyde **53** incubated with

Table 5. Semicarbazone Cathepsin K Inhibition

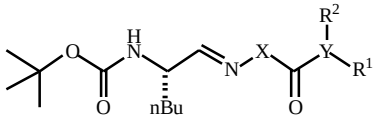

#	X	Y	R^1	R^2	IC_{50} nM
74	NH	N	H	H	350
75	NH	N	Me	H	280
76	NH	N	Et	H	490
77	NH	N	*i*-Pr	H	170
78	NH	N	*t*-Bu	H	160
79	NH	N	Ph	H	400
80	NH	N	$PhCH_2$	H	410
81	NH	N	$Ph(CH_2)_2$	H	260
82	NMe	N	$Ph(CH_2)_2$	H	11,000
83	NH	N	$Ph(CH_2)_2$	Me	45
84	NH	N	Me	Me	72
85	NH	N	Et	Et	40
86	NH	1-pyrrolidine	-	-	36
87	NH	1-piperidine	-	-	58
88	NH	4-morpholine	-	-	35
89	NH	2,3-2H-indole	-	-	48

cathepsin K revealed electron density for the aldehyde **53**, but not the semicarbazide portion. The active site thiol of the protease attacked the aldehyde carbonyl in a similar manner as in the calpeptin derivative structure, with the hydroxyl of the hemithioacetal in the oxyanion hole. As surmised, this structure proved that the *iso*-propyl P^2 group occupied the S^2 pocket, with the *n*-butyl chain making van der Waals interactions with the S^1 wall. The P^3 phenyl moiety inhabits the active site trough, pointing toward the S^3 subsite.

Although these structures provided greater insight into S^1-S^3 subsite preferences which could impact inhibitor design, they raised the possibility that the semicarbazone inhibitors were merely pro-drugs for aldehydes. This hypothesis was supported by the relatively flat SAR and the lack of semicarbazone inhibitors with greater potency than their parent aldehydes. Investigations to test this hypothesis revealed that the semicarbazones, unlike their parent aldehydes, were substantially less active inhibitors of cathepsin K at pH = 7.0 versus pH = 5.5. Finally, ^{13}C NMR experiments with a semicarbazone with cathepsin K gave a resonance corresponding to a hemithioketal adduct with cathepsin K, while no thioaminal resonance was detected between cathepsin K and the semicarbazone. These experiments provided strong support for the semicarbazone pro-drug hypothesis. Since the semicarbazones were likely acting as pro-drugs and did not lead to improvements in potency or selectivity while only modestly improving the inhibitor pharmacokinetic profiles, further efforts in this inhibitor class were curtailed.

CYANAMIDES

Co-current with the directed screen of known serine and cysteine protease inhibitors, a high throughput screen (HTS) of the GlaxoWellcome compound collection was also initiated. In addition to the identification of aldehydes, β-lactones and β-lactams, Michael acceptors, nitriles, α-halomethylketones, diazomethanes, and epoxides, two intriguing hits were identified. The first hit was a library of α-α'-diacylaminoalcohols [175]. These alcohols were inactive upon resynthesis. Surmising that the active species were the ketones, generated from air oxidation after prolonged storage in dimethyl sulfoxide, the corresponding ketones were also prepared. These N-acylated N'-Cbz-valine capped diaminoketones **90** were ~100 nM reversible inhibitors of cathepsin K. Unfortunately, subsequent disclosure of similar inhibitors by SmithKline Beecham [176] later that year led to the abandonment of this series.

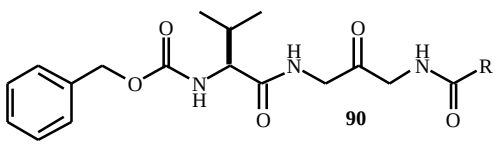

90

Structure 90.

The second interesting HTS hit was a PDE IV inhibitor [177] **91** which was also a reversible and substrate co mpetitive inhibitor of cathepsin K (IC_{50} = 430 nM) [178]. Since nitriles were well documented warheads for cysteine proteases, a hypothesis was formulated that the cyanamide was an important feature of the inhibitor. Stripping away the side chains from the pyrrolidine ring gave the N-pyrrolidinecarbonitrile **92** (IC_{50} = 2,100 nM) which still functioned as a reasonable inhibitor of cathepsin K with only a ~5-fold loss in activity from the starting lead.

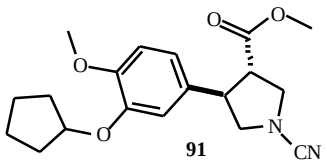

91

Structure 91.

Starting from this key pharmacophore **92**, a strategy was implemented to append substituents to the α or β positions of the pyrrolidine ring to gain binding energy through interactions with the S^2 and S^3 subsites of the enzyme. Borrowing from the aldehyde SAR, the P^2 *tert*-butyl moiety was attached to the pyrrolidine ring. The (S)-proline derived α-series cyanamide **93** (IC_{50} = 60 nM) was 35-fold more potent cathepsin K inhibitor than **92**, while its (R)-proline-derived enantiomer **94** was 5-fold less potent than **93**. Since the enantiomers exhibited significant differences in inhibitory potency, the aza-proline analog **95** was prepared. The aza-proline **95** (IC_{50} = 380 nM) was similar to the (R) enantiomer **94**, and significantly less activity than the (S) proline-derived inhibitor **93**.

In addition to the importance of the α-stereocenter, the ester oxygen was also necessary for maintaining good inhibitory activity as the amide **96** (IC_{50} = 8,100 nM) was over 100-fold less potent than the corresponding ester **93**. Furthermore, the addition of a P^3 element to the cyanamide inhibitor class also enhanced potency. Incorporation of the P^3 group from aldehyde **50** into the cyanamide template resulted in a 30-fold increase in activity for cyanamide **97** (IC_{50} = 1.8 nM) relative to the *tert*-butyl analog **93**.

The effect of ring size on inhibitory activity versus cathepsin K was also explored. As shown in Table **6**, the four-membered aziridine ring was optimal for cathepsin K inhibition. A comparison of the piperidine **98** with pyrrolidine **93** indicates that the six-membered ring is inactive at concentrations up to 13,000 nM. In contrast, the aziridine **99** (IC_{50} = 0.048 nM) is greater than 30-fold more potent than its five-membered ring congener **97**.

In the β-substituted series, the (S)-enantiomer **100** (IC_{50} = 81 nM) was equipotent to the more active α-series analog **93**. In contrast to the α series, the β series (R) enantiomer **101** (IC_{50} = 200 nM) had similar activity to its (S)-enantiomer. Incorporation of a P^3 moiety into the β series also enhanced potency. Thus, analog **102** (IC_{50} = 12 nM) was 6-fold more active than its *tert*-butyl analog **100**, but less potent than its corresponding α series analog **97**.

X-ray co-crystal structures of aldehyde inhibitors with cathepsin K revealed a key hydrogen bond between the carbamate NH of the inhibitor and ^{161}Asn of the enzyme [170,169]. These cyclic cyanamides of the α series are incapable of forming a similar interaction. Speculating that

Table 6. Cyclic Cyanamides Cathepsin K Inhibition

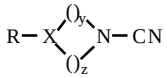

#	R	X	y	z	IC_{50} nM
91					430
92	H	CH	3	0	2,100
93	*t*-BuO(C=O)	(S)-CH	3	0	60
94	*t*-BuO(C=O)	(R)-CH	3	0	300
95	*t*-BuO(C=O)	N	3	0	380
96	*t*-BuNH(C=O)	(S)-CH	3	0	8,100
97	(S)-$CyCH_2CH(Me)O(C=O)$	(S)-CH	3	0	1.8
98	*t*-BuO(C=O)	(S)-CH	4	0	>13,000
99	(S)-$CyCH_2CH(Me)O(C=O)$	(S)-CH	2	0	0.048
100	*t*-BuO(C=O)NH	(S)-CH	1	2	81
101	*t*-BuO(C=O)NH	(R)-CH	1	2	200
102	(S)-$CyCH_2CH(Me)O(C=O)NH$	(S)-CH	1	2	12
103	Cbz-Leu-NH	CH	1	2	19

additional binding energy could be obtained by introducing such an interaction, this hypothesis was investigated [179]. The acyclic cyanamides **104** and **105** were prepared to avoid the conformation bias imposed by the ring. A comparison of the methylene acyclic cyanamide **104** (IC_{50} = 26 nM) which lacks a hydrogen bond donor to the aza-cyanamide **105** (IC_{50} = 0.009 nM) that contains a hydrogen bond donor revealed that the hydrogen bond donor analog was over three orders of magnitude more potent, even though the methylene acyclic cyanamide **104** was still a effective cathepsin K inhibitor. To further explore this hydrogen bond hypothesis, the methyl analogs **106**, **107**, and **108** were prepared. The N-methyl derivative **106** (IC_{50} = 62 nM) had similar inhibitory activity to the methylene analog **104**, while the (S)-methyl analog **107** (IC_{50} = 2,300 nM) and the (R)-methyl analog **108** (IC_{50} = >13,000 nM) were substantially less active. These results supported the hypothesis than the carbamate NH of **105** forms a hydrogen bond interaction with ^{161}Asn. In addition to the hydrogen bond, the slightly different conformation of the inhibitor arising from the sp^2 geometry of the carbamate nitrogen may also contribute to the large increase in inhibitory potency of the azacyanamide **105**. The sp^3 orientation of substituents attached to the α-carbons of esters **104**, **107**, and **108** may be poorly accommodated by the protein. Regardless of the orientation of substituents at this position, there appears to be little room for alkyl groups (Compare **104** to **107** and **108** or **105** to **106**).

Desiring to make a direct comparison of the cyanamide warhead to a nitrile warhead, cyanides **109**, **110**, and **111** were prepared. The nitrile **109** (IC_{50} = 7,900 nM) was over five orders of magnitude less potent than the cyanamide **105**, and the α-methyl nitriles **110** and **111** were even poorer inhibitors of cathepsin K. The greater electrophilicity of the cyanamide warhead accounts for most of this difference, but the sp^2 geometry of the cyanamide may also afford a better fit with the enzyme.

The amide **112** (IC_{50} = 830 nM) was also synthesized. It was 30-fold less potent than the ester **104**. This result was similar to the cyclic cyanamide analog **96** underscoring the detrimental effect of a sp^2 amide nitrogen relative to a sp^3 orientation at this position. The higher penalty to desolvate a NH versus an O may also contribute to the loss in inhibitory activity.

The effect of P^1 substituents on enzyme inhibition was also explored. Qualitatively, the P^1 SAR paralleled the results of the aldehyde inhibitors from Table **1**. Increased steric bulk adjacent to the cyanamide decreased inhibitor potency (Compare **113** to **114** and **115**). In contrast, branching farther down the P^1 chain was better tolerated (Compare **117** or **119** to **118** or **120**).

As shown in Table **8**, these inhibitors were quite selectivity versus the aminopeptidase cathepsin H [179,178]. In contrast, they were good inhibitors of the closely related endoprotease cathepsin L, with the selectivity against the carboxypeptidase cathepsin B being moderate. In general, the nitrile **104**, although being less potent than the cyanamides, was more selective than the much more electrophilic cyanamides.

Table 7. Acyclic Cyanamide Cathepsin K Inhibition

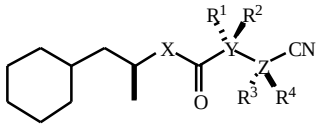

#	X	Y	R^1	R^2	Z	R^3	R^4	IC_{50} nM
104	O	C	H	H	N	Me	---	26
105	O	N	H	---	N	Me	---	0.009
106	O	N	Me	---	N	Me	---	62
107	O	C	Me	H	N	Me	---	2,300
108	O	C	H	Me	N	Me	---	>13,000
109	O	N	H	---	C	H	H	7,900
110	O	N	H	---	C	Me	H	>13,000
111	O	N	H	---	C	H	Me	>13,000
112	NH	C	H	H	N	Me	---	830
113	O	N	H	---	N	Et	---	0.003
114	O	N	H	---	N	*i*-Pr	---	0.019
115	O	N	H	---	N	*t*-Bu	---	1,500
116	O	N	H	---	N	Cy	---	0.016
117	O	N	H	---	N	*n*-Pr	---	0.004
118	O	N	H	---	N	*i*-Bu	---	0.004
119	O	N	H	---	N	*n*-Bu	---	0.007
120	O	N	H	---	N	Bn	---	0.006

Table 8. Cyanamide Cathepsin B, H, K, and L Inhibition and Selectivity

#	Cat K IC_{50} nM	Cat B IC_{50} nM	Cat H IC_{50} nM	Cat L IC_{50} nM
97	1.8	310	580	130
99	0.048	2.4	40	0.71
102	12	680	8,300	81
104	26	2,600	>13,000	1,500
105	0.009	0.077	1.4	0.025
114	0.019	1.3	0.46	0.79

As shown in Figure (**1B**), a X-ray co-crystal structure of *t*-BuO(C=O)NHN(Me)CN with cathepsin K helped confirm molecular modelling predictions. The cathepsin K active site thiol of ^{25}Cys forms a covalent isothiourea intermediate with the cyanamide moiety of the inhibitor. Additionally, two hydrogen bonds from the backbone NH of ^{25}Cys and the side chain carbonyl oxygen of ^{19}Gln stabilize the NH of the isothiourea. Moreover, the S^2 pocket formed by residues ^{67}Tyr, ^{68}Met, ^{134}Ala, ^{163}Ala, and ^{209}Leu is inhabited by the *tert*-butyl P^2 fragment. Furthermore, the backbone NH of ^{66}Gly donates a hydrogen atom to the carbonyl oxygen of the carbamate, while the backbone carbonyl oxygen of ^{161}Asn accepts a hydrogen atom from the carbamate NH of the inhibitor. Finally, the P^1 methyl group points down the S^1 groove comprised of ^{23}Gly, ^{24}Ser, ^{64}Gly, and ^{65}Gly. The acyclic, aza-cyanamide inhibitors are virtually superimposable on the corresponding aldehyde inhibitor structures, as shown for aldehyde **53** in Figure (**1B**), underscoring the similar binding modes of these two inhibitor classes.

The acyclic aza-cyanamides were rapidly metabolized by S9 liver preparations, whereas the pyrrolidine cyanamides were relatively stable [180]. Furthermore, the aza-cyanamides were rapidly degraded in plasma, probably owing to their excellent electrophilicity. In spite of these liabilities, several aza-cyanamides were able to attenuate bone resorption in the rat calvarial resorption assay. Further work in this series could possibly lead to developable drug

candidates, but with limited resources, efforts were shifted to the more promising ketoamide series.

KETOHETEROCYCLES

In addition to the warheads described above, these laboratories also evaluated the use of ketoheterocycles as electrophiles for inhibitors of cathepsin K [181]. The increased metabolic stability of ketoheterocycles versus aldehyde- and semicarbazone-based inhibitors made this approach attractive. In the design of ketoheterocyclic inhibitors, the use of potent P^1, P^2 and P^3 enzyme recognition motifs derived from aldehyde-based inhibitors was expedient. As shown in Table **9**, the unsubstituted thiazole **121** was a low micromolar inhibitor of cathepsin K. Addition of electron withdrawing groups to the thiazole, as in examples **123**-**125**, afforded inhibitors with varying degrees of inhibition with the 4-substituted ester **123** being the most potent analog (IC_{50} = 230 nM). The enhanced potency of analog **123** indicates that there may be a preferred binding mode for the carbonyl group to the enzyme. Replacement of the chiral P^2 moiety in the ketothiophene **126** with an achiral symmetrical P^2 piece afforded an equipotent inhibitor (compare **126** to **121**). In addition to these thio-based heterocycles, other aromatic rings were investigated. Furthermore, substitution of alternative P^1 and P^2 groups into these inhibitors were also explored. None of these changes provided more potent analogs than ester **123**. Since other efforts involving ketoamide-based inhibitors were yielding more promising results that seemed to allow exploitation of the aldehyde SAR, it was decided to put more focus on ketoamide-based electrophiles.

KETOAMIDES

Using the norleucine-derived aldehyde lead **2** as a starting point, preliminary efforts to explore ketoamide warhead-based inhibitors focussed on the $S^{1'}$ subsite of cathepsin K [182]. As shown in Table **10**, the prototype ketoamide **127** was substantially less potent than the aldehyde lead. Simple alkyl substituents appended off this amide did not result in additional gains in potency. In addition, incorporation of a more sterically demanding *tert*-butyl group, analog **131**, on the amide resulted in the loss of activity. In order to probe potential π-π stacking interactions with ^{184}Trp on the $S^{1'}$ subsite, various amides with tethered phenyl groups were prepared. While the analog having the benzyl group **133** was fairly active (IC_{50} = 2,900 nM), addition of a α-methyl group to stabilize the active conformation showed the (R)-antipode **135** to be the more potent inhibitor. N-methylation of the (R)-antipode as in **137**, afforded an inactive inhibitor implying the inability of the enzyme to accommodate additional steric bulk in this space.

In the case of aldehyde-based inhibitors, it was observed that probing deeper into the S^2 subsite afforded extremely potent inhibitors such as **46** (IC_{50} = 0.35 nM), **51** (IC_{50} = 0.13 nM), and **58** (IC_{50} = 0.56 nM). As modification in the $P^{1'}$ region afforded fairly modest improvements, it was decided to explore potency enhancing P^2 aldehyde groups in the ketoamide series. As shown in Table **11**, homologation of the *tert*-butyl group in **135** to probe deeper into the S^2 pocket resulted in a 35-fold **139** to 60-fold **140** boost in potency. In addition, with evidence that the S^3 subsite could afford further gains in potency based on the aldehyde SAR, it was decided to append various phenyl linkers off the P^2 backbone of **139**. More than 20- to 30-fold improvements were achieved from additional interactions with the S^3 subsite with the activity residing in the (R)-antipode analogs **141** and **143**. To reduce the synthetic complexity, symmetrical P^2 groups were explored such as analogs **145**-**150**, with analogs **147** (IC_{50} = 2.5 nM) and **149** (IC_{50} = 0.71 nM) being the most active.

Having improved the P^2 moiety of the ketoamide inhibitors, efforts were redirected to the $P^{1'}$ group in order to enhance aqueous solubility [183]. As shown in Table **12**, substitution of the α-methyl benzyl moiety with various heterocycles generally resulted in a loss in activity with the exception of analog **160** (IC_{50} = 1.0 nM). The enhanced potency of analog **160** may arise from a hydrogen bond between the piperidine carbonyl oxygen and the indole NH of ^{184}Trp in the $S^{1'}$ subsite of the enzyme.

Table 9. Ketoheterocycle Cathepsin K Inhibition

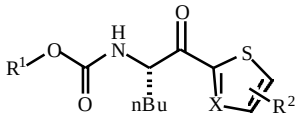

#	R^1	X	R^2	IC_{50} nM
121	(S)-$CyCH_2CH(Me)$	N	H	3,100
122	(S)-$CyCH_2CH(Me)$	N	4-Ph	7,100
123	(S)-$CyCH_2CH(Me)$	N	4-CO_2Et	230
124	(S)-$CyCH_2CH(Me)$	N	4-Me-5-CO_2Et	>10,000
125	(S)-$CyCH_2CH(Me)$	N	4-CF_3	13,000
126	$(i\text{-Pr})_2CH$	C	H	1,900

Table 10. Ketoamide $P^{1'}$ Cathepsin K Inhibition

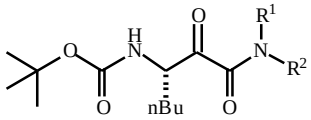

#	R^1	R^2	IC_{50} nM
127	H	H	5,900
128	H	Me	21,000
129	H	Et	18,000
130	H	*i*-Pr	9,100
131	H	*t*-Bu	>100,000
132	H	Ph	6,300
133	H	CH_2Ph	2,900
134	H	$(CH_2)_2Ph$	5,000
135	H	(R)-CH(Me)Ph	1,200
136	H	(S)-CH(Me)Ph	4,200
137	Me	(R)-CH(Me)Ph	>100,000
138	H	CH_2-2-thiophene	3,400

Table 11. Ketoamide P^2-P^3 Cathepsin K Inhibition

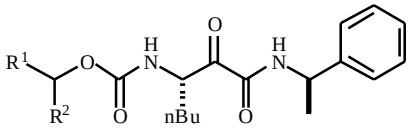

#	R^1	R^2	IC_{50} nM
139	H	*t*-Bu	34
140	Me	*t*-Bu	20
141	$Ph(CH_2)_2$	(R)-*t*-Bu	1.1
142	$Ph(CH_2)_2$	(S)-*t*-Bu	912
143	$Ph(CH_2)_3$	(R)-*t*-Bu	0.79
144	$Ph(CH_2)_3$	(S)-*t*-Bu	1,400
145	Et	Et	76
146	*n*-Pr	*n*-Pr	32
147	*i*-Pr	*i*-Pr	2.5
148	*i*-Bu	*i*-Bu	69
149	*t*-Bu	*t*-Bu	0.71
150	Cp	Cp	6.3

Table 12. Ketoamide $P^{1'}$ Cathepsin K Inhibition

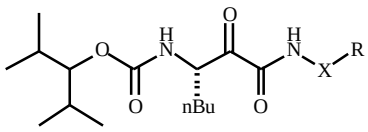

#	X	R	IC_{50} nM
151	CH_2	2-pyridyl	44
152	CH_2	3-pyridyl	23
153	CH_2	4-pyridyl	30
154	CH_2	2-(1,3,4-oxadiazolyl)	19
155	(R)-CH(Me)	2-(1,3,4-oxadiazolyl)	59
156	CH_2	2-thiazolyl	18
157	CH_2	5-thiazolyl	14
158	CH_2	4-thiazolyl	13
159	CH_2	5-isoxazolyl	14
160	---	(S)-3-(2-piperidinonyl)	1.0

As shown in Table **13**, the introduction of heterocyclic moieties into $P^{1'}$ resulted in higher MDCK permeability coefficients, better solubilities, and enhanced oral bioavailability compared to parent compound **147**. The total clearances of analogs **154**, **157**, **159**, and **160** increased relative to **147** ranging from 28-44 mL/min/kg, attenuating gains in absorption.

In addition to methylene linked heterocyclic groups in $P^{1'}$, heterocyclic moieties linked directly to the amide group were also studied as shown in Table **14** [152]. Initial efforts focussed on securing an interaction with ^{184}Trp, which is conserved among the cysteine cathepsins. Various five and six membered heterocycles were studied. The six membered pyridines **161** and **162** were less active than their five membered ring pyrazoles **169** and isoxazoles **168**. Fusion of an additional ring to give the isoquinoline **165** resulted in a boost in potency (IC_{50} = 4.8 nM). In contrast, the site of ring attachment made a difference in activity as the quinoline **164** (IC_{50} = 250 nM) was substantially less active, indicating that favorable π-π stacking interactions with the tryptophan demanded optimal substitution. The five membered heterocycles containing an appropriately displayed hydrogen bond acceptor/donor were generally more potent with the isoxazole **168** (IC_{50} = 5.1 nM) and the pyrazole **169** (IC_{50} = 0.77 nM) being the most potent in this series.

It was tempting to explain these effects based on steric and electronic arguments. Further insights into the binding of these heterocycles and the ketoamide inhibitors in general were first obtained from the X-ray co-crystal structure of compound **169** bound to cathepsin K as shown in Figure (**1D**). Although, the orientation of the P^1 and P^2 groups were in line with modelling predictions, the $P^{1'}$ pyrazole moiety in compound **169**, besides an interaction with the indole of ^{184}Trp, had an additional binding contribution from ^{18}Gln through two water molecules. Another surprising aspect was that the hydroxyl of the hemithioketal was not oriented into the oxyanion hole of the protein. Instead, it interacts with ^{162}His of the catalytic triad, as well as ^{161}Asn, while the amide moiety resides in the oxyanion site. Thus, the active site thiol attacks the electrophile carbonyl group from the opposite face to that observed for previously reported aldehyde and ketone cathepsin K co-crystal structures [150,170,169,174].

With further exploration of the $P^{1'}$ pyrazole group, it was found that the position of a methyl group made a huge difference in terms of potency and selectivity. N-methyl pyrazole **170**, although not as potent due to the loss of a hydrogen bond with ^{184}Trp, was a very selective compound against the other cathepsins (See Table **15**), while N-methyl pyrazole **171** retained its potency with no enhancement of selectivity. Encouraged by these results, a number of $P^{1'}$ N-alkyl/aryl substituted pyrazoles were investigated. Although SAR of the N-alkyl/aryl substitutions was quite flat in terms of potency, large differences in selectivity over the other highly homologous cathepsins were evident with analogs **177** and **179** being >100-fold selective over all the other cathepsins. The N-cycloalkyls were generally more selective than the N-aryl compounds. Steric probes from other positions of the pyrazole such as in analogs **183**-**186** and the constrained indazole **187**, while potent, did not provide any increases in selectivity.

As can be seen in Table **16**, the directly attached $P^{1'}$ heterocyclic compounds had enhanced solubility in fasted state-stimulated intestinal fluid relative to **147** with the pyridine **161** and the pyrazole **169** having the highest solubility. These higher solubilities also led to increased oral

Table 13. Ketoamide P$^{1'}$ Pharmacokinetics Data

#	MDCK P_{APP} nm/sec	Sol. FS-SIF mg/mL	$t_{1/2}$ min	C_l mL/min/kg	V_{SS} mL/kg	F %
147	57	0.012	290	8.7	1,900	3.1
151	510	0.028	77	5.2	240	10
153	---	0.062	240	7.1	90	5.2
154	510	0.15	21	33	980	16
157	480	0.051	150	28	1,300	55
159	410	0.063	52	29	1,200	32
160	310	0.35	220	44	1,600	20

Table 14. Ketoamide P$^{1'}$ Cathepsin K Inhibition

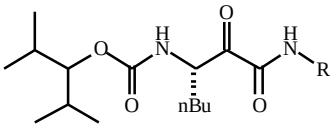

#	R	IC_{50} nM
161	2-pyridyl	32
162	3-pyridyl	95
163	2-pyrazinyl	52
164	2-quinolyl	250
165	2-isoquinolyl	4.8
166	2-thiazolyl	40
167	2-(1,3,4-thiadiazolyl)	83
168	3-isoxazolyl	5.1
169	3-(1H-pyrazolyl)	0.77
170	2-(1-methyl-1H-pyrazolyl)	32
171	3-(1-methyl-1H-pyrazolyl)	0.41
172	2-(1-ethyl-1H-pyrazolyl)	26
173	2-(1-isopropyl-1H-pyrazolyl)	17
174	2-(1-isobutyl-1H-pyrazolyl)	39
175	2-(1-cyclopropylmethyl-1H-pyrazolyl)	27
176	2-(3,3-dimethylbutyl-1H-pyrazole)	62
177	2-(1-cyclobutyl-1H-pyrazolyl)	15
178	2-(1-cyclopentyl-1H-pyrazolyl)	20
179	2-(1-cyclohexyl-1H-pyrazolyl)	22
180	2-(1-phenyl-1H-pyrazolyl)	15
181	2-(4-pyridinyl-1H-pyrazolyl)	25

(Table 14) Contd….

#	R	IC_{50} nM
182	2-(2-pyridinyl-1H-pyrazolyl)	62
183	2-(3-methyl-1H-pyrazolyl)	0.47
184	2-(4-methyl-1H-pyrazolyl)	0.71
185	2-(3-phenyl-1H-pyrazolyl)	0.21
186	2-(4-phenyl-1H-pyrazolyl)	0.65
187	3-(4-fluoro-1H-indazolyl)	0.26

Table 15. Ketoamide Cathepsin B, H, L, S, and V Selectivity

	Cat K IC_{50} nM	B/K	H/K	L/K	S/K	V/K
169	0.77	670	30	40	3.0	21
170	32	>400	>400	250	91	50
171	0.41	>610	ND	56	7.8	29
172	26	>490	>490	220	43	4.2
173	17	>760	>760	260	78	66
174	39	>320	>320	260	59	120
175	27	>470	>470	220	41	63
176	62	>200	>200	68	13	46
177	15	>830	>830	290	130	140
178	20	>630	ND	190	55	71
179	22	>560	>560	190	140	130
180	15	>820	>820	250	69	65
181	25	>500	>500	44	5.4	19
182	62	>200	ND	40	8.3	19
183	0.47	1,100	2,100	26	1.7	14
184	0.71	ND	ND	ND	4.6	ND
185	0.21	1,200	1,700	25	4.1	10
186	0.65	520	18	ND	7.0	20
187	0.26	ND	ND	ND	2.3	ND

bioavailability. Surprisingly, the unsubstituted pyrazole **169** had a higher rate of clearance compared to the N-methyl pyrazole **170**, implying that the methyl group increases metabolic stability.

In addition to modifying $P^{1'}$, it was decided to test the effect of the ketoamide warhead on the P^1 group SAR derived from the aldehyde inhibitors. Like in the aldehyde series, the glycine derived analog **188** (IC_{50} = 12,000) was a weak inhibitor as shown in Table **17**. Increasing the length of the P^1 substituent improved potency. Once again, the *n*-butyl derivative **195** was optimal, and branching in the alkyl chain was better tolerated β, rather than α, to the peptide backbone (Compare **190** and **192** to **191** and **193**).

Simultaneously with the optimization of the P^1 and $P^{1'}$ regions, variations that might afford better P^2 moieties were also pursued. Aaron Miller investigated a structural screening approach [184]. This exploration involved an ACD search of secondary alcohols that were filtered on the basis of size and cost, and then docked into the cathepsin K active site. The 'grow' algorithm within the MVP program was utilized with the active site of cathepsin K fixed during the docking process. Table **18** shows the binding energies

Table 16. Ketoamide P$^{1'}$ Pharmacokinetics Data

#	*c* Log P	Sol. FS-SIF mg/mL	$t_{1/2}$ min	C_l mL/min/kg	V_{ss} L/kg	F %
161	5.0	1.0	130	36	1.2	58
166	4.8	0.074	170	41	3.5	18
167	3.6	0.035	170	28	0.65	15
169	4.6	0.27	700	68	15	41
170	4.6	0.064	240	26	2.0	28

Table 17. Ketoamide P^1 Cathepsin K Inhibition

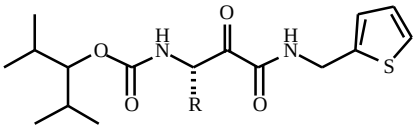

#	R	IC_{50} nM
188	H	12,000
189	Me	360
190	*i*-Pr	47
191	*i*-Bu	24
192	*s*-Bu	87
193	CH_2Cy	14
194	CH_2Ph	27
195	*n*-Bu	9.2

Table 18. Ketoamide P^2 Cathepsin K Inhibition

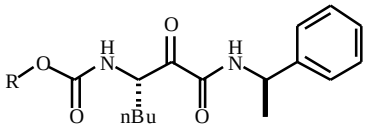

#	R^1	IC_{50} nM	Calc. Bind. Energy
135	*t*-Bu	1,200	-188.5
196	*cis*-3,5-dimethylcyclohexyl	350	-193.7
197	*trans*-3,5-dimethylcyclohexyl	190	-189.7
198	(S)-1-(2,3-dihydroindanyl	100	-193.2
199	(S)-1-(1,2,3,4-tetrahydronaphthalyl)	32	-194.2
200	norborneolyl	26	-190.5

(Table 18) Contd….

#	R^1	IC_{50} nM	Calc. Bind. Energy
201	fenchyl	5.7	-175.4
202	adamantanyl	7.2	-176.2
203	(S)-pantolactonyl	3.0	-194.5
204	(S)-pantolactamyl	2.5	---

obtained from the docking procedure, as well as the inhibitory potencies versus cathepsin K. The P^2 moieties that exhibited good calculated binding energies relative to the starting *tert*-butyl group were selected for synthesis. As can be seen in Table **18**, all the virtual screening analogs synthesized afforded potent cathepsin K inhibitors. Although hydrophobicity played a role in some cases such as analogs **200**-**202**, the presence of a hydrogen bond as in **203** between the lactone carbonyl and the backbone NH of ^{66}Gly in cathepsin K, as suggested by the docking calculations, also allowed for the accommodation of small P^2 groups with better potency. There was no correlation between the calculated binding energies and the measured inhibition constants. Such a disconnect could be due to the static nature of the protein active site model that did not allow for conformational changes in the subsites to accommodate larger substituents in the P^2 pocket. As shown in Table **19**, these analogs were quite selective versus the exopeptidase cathepsins B and H, with good selectivity versus endoproteases cathepsins L and V, and moderate selectivity versus cathepsin S.

Of the several more potent cathepsin K inhibitors **201**-**203**, analog **203** was selected for pharmacokinetic studies since its *c* Log P (5.5) was lower than those of **201** (7.9) and **202** (7.3). As shown in Table **20**, compound **203** had a very high clearance (C_l = 460 mL/min/kg) resulting in a shorter half life ($t_{1/2}$ = 11 min) and no systemic exposure when dosed orally. *In vitro* plasma studies indicated that lactone **203** was rapidly hydrolyzed to the hydroxyl acid. To improve the plasma stability of analog **203**, lactam **204** was synthesized. This modification resulted in a compound that was equipotent to the lactone, but with a lower clearance (C_l = 48 mL/min/kg) and better half life ($t_{1/2}$ = 62 min). In addition, compound **204** had a better systemic exposure after oral dosing.

Since the structural screening approach led to the discovery of a novel and potent inhibitor with reasonable drug properties, it was decided to further investigate the pantolactam **204**. The strategy involved incorporation of a P^3 substituent into the pantolactam template [185,186]. Initially, a combinatorial approach was taken, in which the pyrrolidine derived from reduction of the lactam was coupled to acid chlorides, chloroformates, isocyanates, and sulfonyl chlorides to produce amides, carbamates, ureas, and sulfonamides. As shown in Table **21**, the length of the tether to a P^3 phenyl ring had little effect on inhibitory activity as the one atom linker was similar to the two or three atom linkers (compare **210**, **213** and **216** or **209**, **212**, and **215**). Ultimately, an X-ray crystal structure of analog **220** revealed that the isoxazole P^3 group was solvent exposed, explaining the flat SAR in the tether region. In contrast, the nature of the linkage to the pyrrolidine ring did affect potency. The ureas **210**, **213**, and **216** were more active than the corresponding carbamates **209**, **212**, and **215**, implying that a hydrogen bond donor was important to the ~5-fold increase in activity. The sulfonamide **207** and the amide **208** were also potent inhibitors. As seen in other ketoamide inhibitors, replacement of the $P^{1'}$ phenylethyl moiety with a pyrazole increased potency (compare **217** to **222**). Directly attached aryl rings such as **221** (IC_{50} = 0.81 nM) were also well tolerated.

As shown in Table **22**, these pantolactam derived inhibitors were quite selective against the cathepsin exopeptidases B and H, and good selectivity was obtained versus cathepsins L and V for several inhibitors. In contrast, the analogs were only moderately selective versus cathepsin S with carbamate **212** being the most selective.

The pharmacokinetic properties of selected pyrrolidines were determined as shown in Table **23**. Most of the analogs had acceptable solubility in FS-SIF. Several analogs also exhibited excellent permeabilities in the MDCK assay. In contrast, analogs **220** and **222** had moderate permeabilities. The isoxazole **220** had poor systemic exposure after oral dosing, probably reflecting limited absorption as well as a high first pass effect due to its high clearance. Strangely, the analogs with the best solubilities, **220**-**222**, had the lowest oral bioavailabilities, possibly arising from high clearances. Analogs with more moderate clearances and good absorption generally exhibited better oral systemic exposure, with pyridine **219** giving the highest oral exposure.

Co-current with the structural screening work in P^2, efforts to modify the P^2 moiety of analogs like **141** and **143** to decrease synthetic complexity were pursued [187]. As shown in Table **24**, inhibitor design involved replacing the *tert*-butyl group with achiral groups. The *gem* dimethyl analog **223** (IC_{50} = 630 nM) and the cyclobutyl analog **224** (IC_{50} = 710 nM) were moderate inhibitors of cathepsin K. Since the S^2 subsite is a fairly hydrophobic pocket, increasing the size of the P^2 moiety, as in analogs **225**-**227**, to increase lipophilic contacts resulted in a 3-25-fold boost in potency.

For optimal S^2 binding, molecular modelling studies indicated that addition of a methylene spacer could help put the P^2 group deeper into the S^2 pocket. This methylene extension resulted in a ~10-fold increase in inhibitory

Table 19. Ketoamide Cathepsin K, B, H, L, S, and V Inhibition

#	Cat K IC_{50} nM	Cat B IC_{50} nM	Cat H IC_{50} nM	Cat L IC_{50} nM	Cat S IC_{50} nM	Cat V IC_{50} nM
196	350	>13,000	>13,000	4,400	63	2,800
197	190	>13,000	>13,000	6,800	290	2,000
198	100	>13,000	>13,000	460	280	290
199	32	>2,000	>2,000	660	79	340
200	26	>13,000	>13,000	1,000	19	190
201	5.7	12,000	>13,000	1,700	30	180
202	7.2	>5,000	>5,000	2,600	16	390
203	3.0	>500	>500	410	13	79
204	2.5	1,400	>13,000	150	18	29

Table 20. Ketoamide P^2 Pharmacokinetics Data

#	*c* Log P	Sol. FS-SIF mg/mL	$t_{1/2}$ min	C_l mL/min/kg	V_{SS} mL/kg	F %
203	5.5	0.24	11	460	3400	0
204	4.6	0.80	62	48	1300	25

Table 21. Ketoamide P^3 Cathepsin K Inhibition

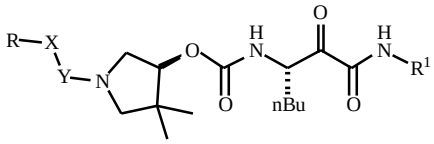

#	R	X	Y	R^1	IC_{50} nM
205	Ph	---	CH_2	(R)-CH(Me)Ph	21
206	Ph	---	CO	(R)-CH(Me)Ph	65
207	Ph	---	SO_2	(R)-CH(Me)Ph	8.3
208	Ph	CH_2	CO	(R)-CH(Me)Ph	3.0
209	Ph	O	CO	(R)-CH(Me)Ph	29
210	Ph	NH	CO	(R)-CH(Me)Ph	4.3
211	Ph	CH_2	SO_2	(R)-CH(Me)Ph	17
212	$PhCH_2$	O	CO	(R)-CH(Me)Ph	24
213	$PhCH_2$	NH	CO	(R)-CH(Me)Ph	3.8
214	$Ph(CH_2)_2$	CH_2	CO	(R)-CH(Me)Ph	27
215	$Ph(CH_2)_2$	O	CO	(R)-CH(Me)Ph	32
216	$Ph(CH_2)_2$	NH	CO	(R)-CH(Me)Ph	6.6

(Table 21) Contd….

#	R	X	Y	R^1	IC_{50} nM
217	4-CF_3-Ph	NH	CO	(R)-CH(Me)Ph	2.1
218	Morpholino	---	CO	(R)-CH(Me)Ph	16
219	3-pyridyl	---	CO	(R)-CH(Me)Ph	14
220	4-(3,5-Me_2-isoxazolyl)	NH	CO	(R)-CH(Me)Ph	15
221	2-benzthiazolyl	---	---	3-pyrazole	0.81
222	4-CF_3-Ph	NH	CO	3-pyrazole	0.42

Table 22. Ketoamide Cathepsin B, H, L, S, and V Selectivity

#	B/K	H/K	L/K	S/K	V/K
207	7,100	>13,000	74	16	79
208	4,300	>13,000	76	17	140
210	2,900	>13,000	1,400	45	120
211	5,200	>13,000	910	12	79
212	>10,000	>10,000	1,300	83	170
213	4,600	>13,000	1,200	46	130
216	5,200	>13,000	760	26	85
217	>120	>120	>120	11	43
218	210	>800	81	2.8	15
219	360	>890	52	4	11
220	270	>810	39	3	9
221	>310	>310	>310	7	32
222	>600	>600	>600	7	36

Table 23. Pantolactam Derivative Ketoamide Pharmacokinetics Data

#	MDCK P_{APP} nm/sec	Sol. FS-SIF mg/mL	$t_{1/2}$ min	C_l mL/min/kg	V_{SS} mL/kg	F %
207	---	---	150	27	2100	25
208	410	0.068	63	26	1500	29
213	210	0.053	61	32	1400	21
219	210	0.085	94	34	550	45
220	12	0.32	35	83	1400	8.8
221	250	0.16	180	65	2200	14
222	18	0.14	75	77	2600	26

activity (compare **223** to **228**), reinforcing the modelling hypothesis. In addition, modelling studies also suggested that addition of a methylene spacer between P^2 and P^3 would enhance binding interactions with the S^3 subsite. To confirm this speculation, analog **229** was synthesized, the addition of a methylene was found to enhance the potency by another 5-fold over analog **228**. Constrained analogs of **229**, such as **230** and **231**, did not offer any additional boost in potency. Since extension of the chain as in analogs **141** (IC_{50} = 1.1 nM) and **143** (IC_{50} = 0.79 nM) afforded potent inhibitors of cathepsin K, similar modifications afforded compounds **232** (IC_{50} = 24 nM) and **233** (IC_{50} = 17 nM), but no additional gain in potency resulted, possibly due to higher entropic costs for binding.

Although potent compounds resulted from this work, there were solubility concerns due to the increasing lipophilicity of these inhibitors. Utilizing P^1 and $P^{1'}$ SAR from previous ketoamide inhibitors to design better inhibitors, hydrophilic groups were substituted singly or in combination at these positions (See Table **25**). The pyrazole analog **234** (IC_{50} = 0.83 nM) was an extremely potent inhibitor compared with analog **230** (IC_{50} = 8.5 nM). Addition of water solubilizing groups at P^1 as in analogs **236** and **237** did not affect the overall potency versus **230**. Furthermore, substitution of a pyridine group at $P^{1'}$ along with a substituted lysine at P^1 resulted in about 5-fold loss in potency when compared to **230**.

Representative examples from this series with $P^{1'}$, P^2 and P^3 modifications were also profiled in a selectivity panel as shown in Table **26**. Although selectivity against exopeptidases B and H was easily achievable, and good selectivity was obtained versus cathepsin L, the analogs were only moderately selective versus cathepsin S.

A number of analogs containing water solubilizing groups were profiled in male Han- Wistar rats for pharmacokinetic parameters as shown in Table **27**. All compounds had good permeability values with the exception of analog **238** (P_{APP} = 14 nm/sec). Analogs **235** (FS-SIF Sol. = 0.032 mg/mL) and **236** (FS-SIF Sol. = 0.027 mg/mL) had poor solubility in FS-SIF resulting in poor oral exposure. In contrast, analogs **234** (FS-SIF Sol. = 0.15 mg/mL) and **237** (FS-SIF Sol. = 0.098 mg/mL) had better FS-SIF solubilities than analogs **235** and **236** and this property might be reflective of their better oral bioavailability. Analog **238**, although being twice as soluble as analog **234**, had poor oral systemic exposure, underscoring the importance of membrane permeability for oral bioavailability.

As shown in Figure (**1C**), further insights into the binding of these inhibitors were derived from an X-ray co-crystal structure of cathepsin K with analog **234**. As in the X-ray co-crystal structure of analog **169** described previously, quite similar binding modes were observed with the S^1 subsite and the active site thiol. Also, as expected, the $P^{1'}$ pyrazole formed a hydrogen bond with the indole NH of ^{184}Trp. In contrast to the *iso*-propyl group of **169**, the cyclobutyl moiety of **234** does not fit as deeply into the S^2 pocket. Its larger P^3 phenyl group does extend farther up the active site trough toward the S^3 subsite, partially compensating for this less favorable habitation of the S^2 subsite.

With the incorporation of $P^{1'}$ heterocycles affording selective inhibitors of cathepsin K over other highly homologous cathepsins, concomitant efforts were directed towards combining optimal selectivity enhancing $P^{1'}$ moieties with potent P^2/P^3 groups in the hope of obtaining additional gains in potency and/or selectivity due to differences in steric requirements in the S^2 subsites of cathepsins K, L, S, and V. As shown in Table **28**, incorporation of non-selective $P^{1'}$ groups with a P^2/P^3 *gem* dimethyl group as in analogs **239**, **240**, and **242** afforded fairly potent inhibitors with analog **240** being the most potent (IC_{50} = 1.6 nM) [188]. As expected from previous work, incorporation of $P^{1'}$ unsubstituted pyrazoles as in analogs **240**, **244**, **249**, **253**, and **257** provided the most potent cathepsin K inhibitors. Addition of α−N-methyl pyrazole as in analog **241** (IC_{50} = 1200 nM) resulted in a dramatic loss in potency, probably resulting from the loss of a hydrogen bond to the indole of ^{184}Trp. Reaching deeper into the hydrophobic S^2 subsite by the use of constrained analogs such as cyclobutyl and cyclopentyl resulted in enhancements in potency. Furthermore, inclusion of heteroatoms in P^2 as in analogs **248**-**251** was not detrimental to the enzyme activity. Although some loss in potency by the N-methylation of the $P^{1'}$ pyrazole was expected (compare **245** to **244** and **254** to **253**), the complete loss in activity of analog **258** versus **257** suggested that accommodation by one subsite resulted in shifts in binding at other subsites that were less favorable for binding to cathepsin K.

A quick look at the selectivity profile of pyrazoles containing varied P^2/P^3 moieties is shown in Table **29**. There was no gain in selectivity from steric differences in these P^2/P^3 groups, despite the literature precedent that steric differences in the S^2 pocket can be exploited for enhanced cathepsin K selectivity [154]. These inhibitors have a carbamate linker that forces the P^2 substituent one atom further away than the corresponding dipeptide-based inhibitors, resulting in altered binding conformations which could influence their selectivity.

Knowing from previous work (See Table **15**) that N-substitution of the pyrazole moiety can result in more selective cathepsin K inhibitors, it was gratifying to find that changes in the P^2/P^3 group, along with N-methyl pyrazole in the $P^{1'}$ region, afforded a fairly potent and selective cathepsin K inhibitor **245**. Thus, a number of N-substituted pyrazole analogs were prepared as shown in table **28** (see analogs **262**-**271**). Although the potency of these analogs was generally comparable, there were significant differences in selectivity between them and the unsubstituted pyrazole **244**. Interestingly when compared to analogs having an isopropyl P^2/P^3 substituent **177** (IC_{50} = 15 nM) and **179** (IC_{50} = 22 nM) with over a 100-fold selective for cathepsins B, H, L, S and V, the cyclobutyl P^2/P^3 analogs **268** (IC_{50} = 45 nM) and **270** (IC_{50} = 58 nM) are considerably less selective versus cathepsins S and V. Analogs **245** and **262** were amongst the most selective inhibitors for this P^2/P^3 cyclobutyl series. Although the $S^{1'}$ subsite of these enzymes are very similar, it is interesting to note that changes in the $P^{1'}$ substituents can effect selectivity of these inhibitors.

Having explored modifications in the P^2/P^3 regions coupled with $P^{1'}$ heterocycles that resulted in selective

Table 24. Ketoamide P^2-P^3 Cathepsin K Inhibition

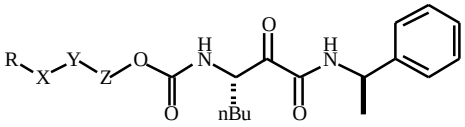

#	R	X	Y	Z	IC_{50} nM
223	Ph	CH_2	$C(Me)_2$	---	630
224	Ph	CH_2	Cb	---	710
225	Ph	CH_2	Cp	---	25
226	Ph	CH_2	$C(Et)_2$	---	150
227	Ph	CH_2	Cy	---	210
228	Ph	---	$C(Me)_2$	CH_2	65
229	Ph	CH_2	$C(Me)_2$	CH_2	13
230	Ph	CH_2	Cb	CH_2	8.5
231	Ph	CH_2	Cp	CH_2	26
232	Ph	$(CH_2)_2$	Cb	CH_2	24
233	Ph	$(CH_2)_3$	Cb	CH_2	17

Table 25. Combination Ketoamide Cathepsin K Inhibition

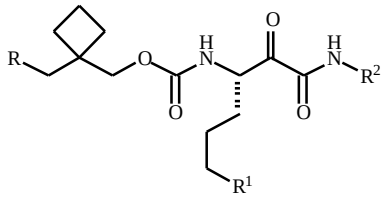

#	R	R^1	R^2	IC_{50} nM
234	4-F-Ph	H	3-pyrazolyl	0.83
235	4-F-Ph	Me_2NSO_2NH	CH_2-3-Py	40
236	2-F,6-F-Ph	MeNHCONH	(S)-CH(Me)Ph	24
237	4-F-Ph	MorpholinoCONH	(S)-CH(Me)Ph	13
238	4-Py	MorpholinoCONH	(S)-CH(Me)Ph	7.6

Table 26. Ketoamide Cathepsin B, H, L, and S Inhibition

#	Cat B IC_{50} nM	Cat H IC_{50} nM	Cat L IC_{50} nM	Cat S IC_{50} nM
225	> 12,000	> 12,000	3,000	430
228	> 5,000	> 5,000	3,000	270
229	> 5,000	> 5,000	1,200	20
230	3,600	> 5,000	1,300	20

(Table 26) Contd….

#	Cat B IC_{50} nM	Cat H IC_{50} nM	Cat L IC_{50} nM	Cat S IC_{50} nM
231	> 5,000	> 5,000	2,200	11
232	> 2,000	> 2,000	1,600	34
233	> 2,000	> 2,000	1,300	17
234	> 500	>500	330	5.2
235	> 5,000	> 5,000	> 5,000	130
237	> 5,000	> 5,000	680	27

Table 27. Combination Ketoamide Pharmacokinetics Data

#	MDCK P_{APP} nm/sec	Sol. FS-SIF mg/mL	$t_{1/2}$ min	C_l mL/min/kg	V_{SS} mL/kg	F %
234	150	0.15	120	45	---	31
235	69	0.032	270	9.6	420	18
236	140	0.027	94	33	1600	15
237	470	0.098	110	43	4200	38
238	14	0.30	74	27	660	8.1

Table 28. Ketoamide P^2 and $P^{1'}$ Cathepsin K Inhibition

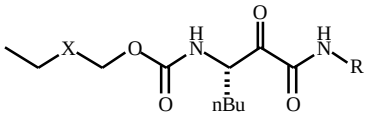

#	X	R	IC_{50} nM
239	$C(Me)_2$	(R)-CH(Me)Ph	36
240	$C(Me)_2$	2-(1H-pyrazolyl)	1.6
241	$C(Me)_2$	2-(1-methyl-1H-pyrazolyl)	1200
242	$C(Me)_2$	3-isoxazolyl	25
243	Cb	(R)-CH(Me)Ph	71
244	Cb	2-(1H-pyrazolyl)	1.9
245	Cb	2-(1-methyl-1H-pyrazolyl)	62
246	Cb	2-(4-phenyl-1H-pyrazolyl)	6.2
247	Cb	3-isoxazolyl	20
248	CH_2OCH_2	(R)-CH(Me)Ph	68
249	CH_2OCH_2	2-(1H-pyrazolyl)	17

(Table 28) Contd….

#	X	R	IC_{50} nM
250	CH_2OCH_2	3-isoxazolyl	350
251	CH_2OCH_2	2-(4-phenyl-1H-pyrazolyl)	10
252	Cp	(R)-CH(Me)Ph	68
253	Cp	2-(1H-pyrazolyl)	1.8
254	Cp	2-(1-methyl-1H-pyrazolyl)	135
255	Cp	2-(4-phenyl-1H-pyrazolyl)	22
256	Ch	(R)-CH(Me)Ph	140
257	Ch	2-(1H-pyrazolyl)	18
258	Ch	2-(1-methyl-1H-pyrazolyl)	>12000
259	Ch	3-isoxazolyl	120
260	Ch	3-(6-chloro-1H-indazolyl)	1.6
261	Cb	3-(1-methyl-1H-pyrazolyl)	3.4
262	Cb	2-(1-ethyl-1H-pyrazolyl)	52
263	Cb	2-(1-isopropyl-1H-pyrazolyl)	54
264	Cb	2-(1-isobutyl-1H-pyrazolyl)	76
265	Cb	2-(1-cyclopropylmethyl-1H-pyrazolyl)	51
266	Cb	2-(1-benzyl-1H-pyrazolyl)	65
267	Cb	2-(3,3-dimethylbutyl-1H-Pyrazolyl)	71
268	Cb	2-(1-cyclobutyl-1H-pyrazolyl)	45
269	Cb	2-(1-cyclopentyl-1H-pyrazolyl)	83
270	Cb	2-(1-cyclohexyl-1H-pyrazolyl)	58
271	Cb	2-(1-phenyl-1H-pyrazolyl)	63

Table 29. Ketoamide Cathepsin L, S, and V Inhibition

#	Cat L IC_{50} nM	Cat S IC_{50} nM	Cat V IC_{50} nM
240	----	1.6	----
244	37	1.4	10
245	12,600	4,000	9,300
246	----	11	----
253	54	1.8	15
257	----	5.9	----
260	11	1.3	5.2

Table 30. Ketoamide Cathepsin B, H, L, S, and V Selectivity

#	B/K	H/K	L/K	S/K	V/K
245	>200	>200	>200	65	150
261	3700	3700	38	1.3	8.5
262	>240	>240	>240	44	89
263	>230	>230	>230	30	65
264	>170	>170	>170	14	89
265	>250	>250	>250	33	102
266	>200	>200	130	7.2	34
267	>180	>180	160	10	43
268	>280	>280	270	14	49
269	>150	>150	130	8.5	32
270	>220	>220	150	10	33
271	>200	>200	240	33	62

cathepsin K inhibitors irrespective of the P^2 moiety, efforts were then directed towards extension of the side chain on the P^2 cyclobutyl moiety to potentially interact with ^{67}Tyr in the S^3 subsite, possibly enhancing the potency, selectivity, and/or physiochemical properties of this class of inhibitors. As shown in Table **31**, N-methyl-imidazole analog **272** (IC_{50} = 61 nM) with reduced conformational flexibility was more potent than its flexible counterparts **273** and **274** [189]. Addition of a phenyl substituent either at the 5- or 1-position in the hope of optimizing a ^{67}Tyr interaction did not result in potency enhancements (see analogs **275** (IC_{50} = 230 nM) and **276** (IC_{50} = 87 nM)). Replacement of the N-methyl imidazole with the thiazole **277** provided a 3.6-fold more potent inhibitor than analog **272**. The increase in potency could be attributed to reduced cost of desolvation to remove associated water molecules or due to more favorable binding interactions in the absence of the methyl substituent. Incorporation of six-membered heterocycles resulted in more potent inhibitors of cathepsin K. The pyrimidine **279** (IC_{50} = 11 nM) as well as the 4-chlorophenyl substituted pyrimidine **280** (IC_{50} = 9.5 nM) analogs were well tolerated relative to imidazoles **272** and **276**.

The oxygen linked analogs **281**-**291** were also profiled. Although the thiazole incorporation afforded an equipotent inhibitor (see **281** and **277**), the heteroatom substitution in the P^3 pyrimidine inhibitors (compare **282** to **279**) resulted in a 23-fold loss in potency. Attachment of the oxygen linker to the 4-position of the pyrimidine gave analog **283** (IC_{50} = 85 nM). As observed in the five-membered sulfur linked analogs, an increase in conformational flexibility resulted in a loss in potency for compound **284** (IC_{50} >12,000 nM). In the hope of increasing water solubility, analogs **285**-**287** were synthesized and were found to be equipotent inhibitors of cathepsin K. As in the five-membered sulfur linked series, there was no loss in activity on movement of the phenyl ring adjacent to the heteroatom linker (compare **290** and **291** to **275** and **276**). The carbon linked thiazole analogs **292** (IC_{50} = 7.9 nM) and **293** (IC_{50} = 5.5 nM) with less conformational flexibility than **281** were the most potent inhibitors in this heterocyclic cyclobutyl series.

At the same time as the structural screening and synthetic complexity reduction efforts were being investigated, the effect of conformational constraint of the P^2/P^3 linker of analog **143** was also explored [153]. As shown in Table **32**, initial inhibitor design involved replacement of the flexible P^2-P^3 tether with various heterocyclic ring systems in the hope of improving potency, selectivity, and/or pharmacokinetic properties. Analog **294** (IC_{50} = 0.24 nM) was a picomolar inhibitor of cathepsin K that was slightly more potent than compound **143**. Although a higher enthalpic cost is paid to desolvate the water molecules that associate with an oxadiazole ring, the lower entropic cost on constraining the P^2-P^3 tether more than compensates for this enthalpic energy loss. As expected based on previous work, the P^2 (R)-antipode (IC_{50} = 460 nM) was a >1000-fold less active inhibitor of cathepsin K than **294**. Substitution of the *tert*-butyl group with other hydrophobic substituents such as *iso*-propyl **295** (IC_{50} = 0.83 nM) or *tert*-amyl **296** (IC_{50} = 1.5 nM) did not offer any potency advantages. With a preferred P^2 *tert*-butyl substituent in place, substituents in the phenyl P^3 moiety such as *para*-fluoro **297** and *para*-trifluoromethyl **298** were studied primarily to block any metabolism by Cyp^{450} enzymes. As these substitutions did not affect the potency of these inhibitors, they were incorporated into future analog work.

As the $P^{1'}$ aryl group did not offer any solubility enhancement, its replacement with $P^{1'}$ heterocycles offering favorable potency, selectivity, and/or pharmacokinetic characteristics were investigated. Based on previous SAR, incorporation of a $P^{1'}$ pyrazole moiety **299** led to an increase in inhibitory activity versus cathepsin K. Furthermore, the oxadiazole ring was not a unique constraint as other

Table 31. Ketoamide P^3 Cathepsin K Inhibition

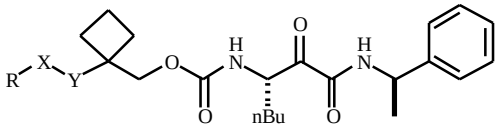

#	R	Y	X	IC_{50} nM
272	2-(1-methyl-1H-imidazolyl)	CH_2	S	61
273	2-(1-methyl-1H-imidazolyl)	$(CH_2)_2$	S	>12000
274	2-(1-methyl-1H-imidazolyl)	$(CH_2)_3$	S	1900
275	2-{5-(4-chlorophenyl)-1-methyl-1H-imidazolyl}	CH_2	S	230
276	2-(1-phenyl-1H-imidazolyl)	CH_2	S	87
277	2-(1,3-thiazolyl)	CH_2	S	17
278	2-(1,3-benzoxazole)	CH_2	S	51
279	2-(pyrimidinyl)	CH_2	S	11
280	2-{4-(4-chlorophenyl)-pyrimidinyl}	CH_2	S	9.5
281	2-(1,3-thiazolyl)	CH_2	O	37
282	2-(pyrimidinyl)	CH_2	O	260
283	4-(2-chloro-pyrimidinyl)	CH_2	O	85
284	4-(2-chloro-pyrimidinyl)	$(CH_2)_3$	O	>12000
285	4-{2-(4-methyl-1-piperazinyl)pyrimidinyl}	CH_2	O	54
286	4-{2-(4-phenyl-1-piperazinyl)pyrimidinyl}	CH_2	O	31
287	4-{2-(4-morpholino-1-piperazinyl)pyrimidinyl}	CH_2	O	54
288	4-(thieno{3,2-d}pyrimidinyl)	CH_2	O	98
289	2-{4-(4-methylphenyl)-1,3-thiazolyl}	CH_2	O	150
290	5-(3-phenyl-1,2,4-thiadiazolyl)	CH_2	O	50
291	3-(6-methyl-4-phenylpyridazinyl)	CH_2	O	57
292	2-(4-trifluoromethyl-1,3-thiazolyl)	CH_2	---	7.9
293	2-(4-phenyl-1,3-thiazolyl)	CH_2	---	5.5

Table 32. Constrained Ketoamide Cathepsin K Inhibition

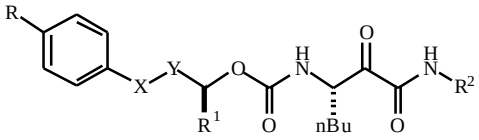

#	R	X	Y	R^1	R^2	IC_{50} nM
294	H	1,3,4-oxadiazole	CH_2	*t*-Bu	(R) CHMePh	0.24
295	H	1,3,4-oxadiazole	CH_2	*i*-Pr	(R) CHMePh	0.83
296	H	1,3,4-oxadiazole	CH_2	*t*-Am	(R) CHMePh	1.5

(Table 32) Contd….

#	R	X	Y	R^1	R^2	IC_{50} nM
297	F	1,3,4-oxadiazole	CH_2	*t*-Bu	(R) CHMePh	0.37
298	CF_3	1,3,4-oxadiazole	CH_2	*t*-Bu	(R) CHMePh	0.41
299	CF_3	1,3,4-oxadiazole	CH_2	*t*-Bu	3-pyrazole	0.029
300	CF_3	1,3-pyrazole	CH_2	*t*-Bu	3-pyrazole	0.072
301	CF_3	1,4-pyrazole	CH_2	*t*-Bu	3-pyrazole	0.032
302	CF_3	1,4-imidazole	CH_2	*t*-Bu	3-pyrazole	0.026
303	CF_3	1,3-imidazolidinone	CH_2	*t*-Bu	3-pyrazole	0.34
304	F	1,3,4-oxadiazole	CH_2	*t*-Bu	2-Me-3-pyrazole	4.9
305	F	1,3,4-oxadiazole	CH_2	*t*-Bu	(S) 3-δ-lactam	0.65
306	F	1,3,4-oxadiazole	CH_2	*t*-Bu	CH_2-3-pyridine	2.8
307	CF_3	1,3,4-oxadiazole	CH_2	*t*-Bu	3-oxazolidinone	0.13
308	CF_3	1,3-pyrazole	CH_2	*t*-Bu	2-pyridine	8.1
309	CF_3	1,4-imidazole	CH_2	*t*-Bu	2-thiazole	5.8
310	CF_3	1,3-pyrazole	CH_2	*t*-Bu	CH_2-5-isoxazole	0.42
311	CF_3	1,3,4-oxadiazole	---	*t*-Bu	3-pyrazole	0.22
312	CF_3	1,3,4-oxadiazole	$(CH_2)_2$	*t*-Bu	3-pyrazole	0.63

heterocyclic rings such as pyrazoles **300** and **301**, imidazole **302**, and 1,3-imidazolidinone **303** could be substituted while maintaining good potency. In addition to the $P^{1'}$ pyrazole, other heterocycles were also substituted into the $P^{1'}$ region of these inhibitors. Gratifyingly, N-methyl pyrazole analog **304** (IC_{50} = 4.9 nM), although less potent, was quite selective over other cysteine proteases (Table **33**). The 2-piperidone **305** (IC_{50} = 0.65 nM), oxadiazolidinone **307** (IC_{50} = 0.13 nM), and the more water soluble pyridines such as **306** (IC_{50} = 2.8 nM) and **308** (IC_{50} = 8.1 nM) were also less active than their corresponding pyrazole containing analogs, presumably due to loss of at least one of the hydrogen bonding interactions. The length of the P^2/P^3 tether was also examined [190]. Both the one atom shorter analog **311** and the one atom longer analog **312** were slightly less active than the lead **299**. But gratifyingly, as shown in Table **33**, the more rigid analog **311** was more selective than **299** or **312**. With the exception of the N-methyl pyrazole derivative **304** and the short tether analog **311**, these inhibitors lacked selectivity versus the cathepsin endopeptidases.

The pharmacokinetic parameters of the constrained analogs are shown in Table **34**. In general, the compounds had quite good MDCK values except for analog **307** (P_{APP} = 15 nm/s), however, this moderate permeability did not limit its oral systemic exposure (F = 79%). Moreover, most of the compounds had good terminal half-lifes ranging from $t_{1/2}$ = 140 min **305** to $t_{1/2}$ = 530 min **299**. The shorter half-life of analog **304** could be attributed to N-demethylation of the pyrazole nitrogen. The cyclic urea **303** was extensively metabolized resulting in a high rate of clearance (C_l = 55 mL/min/Kg). Although some of the analogs were more soluble in FS-SIF compared to other analogs, this plus did not translate to increased systemic exposure upon oral dosing. Thus, solubility of these inhibitors was probably adequate to not seriously influence oral bioavailability. Many of these compounds exhibited excellent pharmacokinetic properties for profiling the pharmacodynamic effects of cathepsin K inhibitors in osteoporotic animal models.

Insights into the binding mode of these constrained heterocyclic ketoamides were obtained by a co-crystal structure of the inhibitor **307** in the active site of cathepsin K as shown in Figure (**1C**). Consistent with the binding of other ketoamides, the amide carbonyl in the oxyanion hole is stabilized by hydrogen bonds to the side chain NH of ^{19}Gln and the backbone NH of ^{25}Cys. As expected, the *n*-butyl P^1 chain occupies the S^1 groove with the *tert*-butyl moiety in the S^2 pocket of the enzyme. Supporting modelling predictions, the $P^{1'}$ oxazolidinone carbonyl oxygen forms a hydrogen bond with the indole NH of ^{184}Trp. Finally, the *para*-trifluoromethyl-phenyl oxadiazole interacts with the active site trough, as well as pointing into the S^3 subsite formed by ^{60}Asn, ^{61}Asp, ^{65}Gly, ^{66}Gly, and ^{67}Tyr.

PHARMACODYNAMIC STUDIES

The *ex vivo* pharmacodynamic properties of representative analogs from several classes of inhibitors were determined in the rat calvaria bone resorption assay, including aldehydes **1**, **46**, and **48**, semicarbazones **86**, **88**, and **89**, cyanamide **105**, and ketoamides **147**, **169**, **299**-**302** [182,152,174,153,179,191]. These inhibitors were all less

Table 33. Ketoamide Cathepsin K, B, L, S, and V Selectivity

#	Cat K IC_{50} nM	Cat B IC_{50} nM	Cat L IC_{50} nM	Cat S IC_{50} nM	Cat V IC_{50} nM
294	0.24	12	10	0.75	1.6
295	0.83	31	17	3.7	5.6
296	1.5	56	17	0.72	2.8
297	0.37	9.8	33	0.53	34
298	0.41	32	190	1.6	5.0
299	0.029	45	69	0.52	1.2
300	0.072	20	8.7	0.21	0.17
301	0.032	10	36	0.078	0.43
302	0.026	27	10	0.16	0.13
303	0.34	60	37	0.54	1.7
304	4.9	3,500	3,800	110	230
305	0.65	6.2	15	0.81	1.3
306	2.8	18	130	2.7	14
307	0.13	5.2	160	1.2	7.1
308	8.1	107	240	3.7	4.5
309	5.8	870	1,000	19	36
310	0.42	23	69	0.12	0.89
311	0.22	29	100	14	20
312	>0.63	>250	240	6.2	5.0

Table 34. Combination Ketoamide Pharmacokinetics Data

#	*c*LogP	MDCK P_{APP} nm/sec	Sol. FS-SIF mg/mL	$t_{1/2}$ min	C_l mL/min/kg	V_{SS} mL/kg	F %
299	3.34	290	0.061	530	11	1900	50
300	5.55	91	0.11	320	9.6	1600	42
301	5.34	120	0.097	340	9.1	2100	45
302	5.08	160	0.13	460	15	2400	55
303	4.80	---	0.043	340	55	5000	27
304	2.59	350	0.058	150	33	3600	88
305	3.10	---	0.62	140	35	1400	17
306	3.53	280	0.49	230	11	1400	46
307	4.42	15	0.17	410	11	3100	79
308	5.96	180	0.38	210	41	1800	34
309	5.33	76	0.048	280	15	1800	43
310	5.99	180	0.064	400	3.2	1700	40

active against the rat ortholog of cathepsin K. For example, ketoamides **300** (rat IC_{50} = 1.3 nM) and **302** (rat IC_{50} = 1.0 nM) are 20-40-fold less potent inhibitors of the rat enzyme than the human enzyme. Mutations in the active site of the rat and human cathepsin K ($^{61}Asp \rightarrow Tyr$ in S^3 and $^{133}Ala \rightarrow Ser$ in S^2) rationalize these results. As expected based on rat cathepsin K IC_{50}s, the various inhibitor classes were significantly less potent in attenuating deoxypyridinoline crosslink release in the *ex vivo* rat calvarial resorption assay (IC_{50} = 100-10,000 nM) [192,193].

Subsequent to the early inhibitor discovery efforts, a human osteoclast assay was also set-up [194]. Human peripheral blood monocyte cells were differentiated into osteoclast-like cells by placement on bone chips in media followed by treatment with RANK-L and M-CSF. Then, comparisons of calcium release into media during bone resorption were made between vehicle and a cathepsin K inhibitor. Several ketoamides were assayed, including **299** (IC_{50} = 690 nM), **300** (IC_{50} = 120 nM), **301** (IC_{50} = 190 nM), and **302** (IC_{50} = 570 nM) [153]. These ketoamide were an order of magnitude more active in the human osteoclast assay than the rat calvaria assay.

Furthermore, two ketoamides were tested in an *ex vivo* osteoarthritis model, the bovine cartilage plug assay [195]. Cylindrical articular cartilage cored from bovine patellae is placed in media and treated with IL-1β, to stimulate protease-induced cartilage degradation, with or without inhibitor. Subsequently, proteoglycan or hydroxyproline concentrations in the media are compared. Ketoamides **147** and **304** were able to attenuate proteoglycan and hydroxyproline release at 10,000 nM in this osteoarthritic model [196].

In spite of this species-specific loss in inhibitory activity, several ketoamides were tested in an *in vivo* model of osteoporosis, the thyroid-parathyroidectomized hypocalcemic rat assay (TPTX) [197]. The data for two of these inhibitors is shown in Table **35**. In this model, PTH secretion is prevented by removal of the parathyroid gland, altering maintenance of calcium homeostasis *via* PTH-stimulated bone resorption. Then, sources of dietary calcium supplementation are eliminated, resulting in rapid depletion of serum calcium. A rapid recovery in serum calcium levels can be achieved by infusion of hPTH (1-34) @ 30,000 ng/kg/h. The PTH-stimulated calcium increase in this model can be dose-dependently attenuated by oral administration of cathepsin K inhibitors **300** or **302** which block collagen matrix degradation after the initial removal of the top layer of hydroxyapatite [153]. Statistical significance was reached at the 100 mg/kg p.o. dose. In addition to the calcium released from the bone surface *via* mineral dissolution to expose collagen fibrils, additional sources of serum calcium could arise from compensation for the attenuation of cathepsin K activity by osteoblastic MMP-13 and MMP-14 [198]. In spite of these counteractions, treatment of the rats with cathepsin K inhibitors clearly inhibited calcium release from bone in this very severe osteoporotic model.

SUMMARY

Desiring to develop new therapeutics for the treatment of osteoporosis, a novel target, cathepsin K, was chosen and aldehyde and cyanamide leads were discovered through directed and high throughput screening, respectively. Rapid SAR development in the aldehyde series led to X-ray structural data. This SAR and structural information were applied to the cyanamide series, as well as new series derived from warhead substitution, including semicarbazone, ketoamide, and ketoheterocycle classes. After preliminary explorations of these series, the ketoamide inhibitors were selected as the most promising series based on potency, selectivity, and pharmacokinetic criteria. Modifications to $P^{1'}$, P^2, and P^3 resulted in potency and selectivity improvements as well as acceptable oral exposure. Combinations of these changes coupled with conformational constraint of the P^2-P^3 linker afforded picomolar cathepsin K

Table 35. Ketoamide rat TPTX Hypocalcemic Resorption Assay

t hr		Serum Calcium					
		Veh.	**PTH**	**300 30[a]**	**300 100[a]**	**302 30[a]**	**302 100[a]**
0	Avg.	1.07	1.07	1.05	1.07	1.12	1.14
	S. D.	0.07	0.06	0.10	0.04	0.08	0.09
2	Avg.	0.98	1.19	1.14	1.10	1.21	1.16
	S. D.	0.03	0.08	0.13	0.03	0.09	0.06
4	Avg.	0.94	1.41	1.30	1.21[c]	1.42	1.31[b]
	S. D.	0.06	0.06	0.07	0.02	0.05	0.07
6	Avg.	0.90	1.64	1.57	1.34[c]	1.63	1.51[b]
	S. D.	0.04	0.04	0.20	0.07	0.04	0.07

[a]Dose, mg/kg

[b]$p < 0.05$ to compared PTH control

[c]$p < 0.01$ to compared PTH control

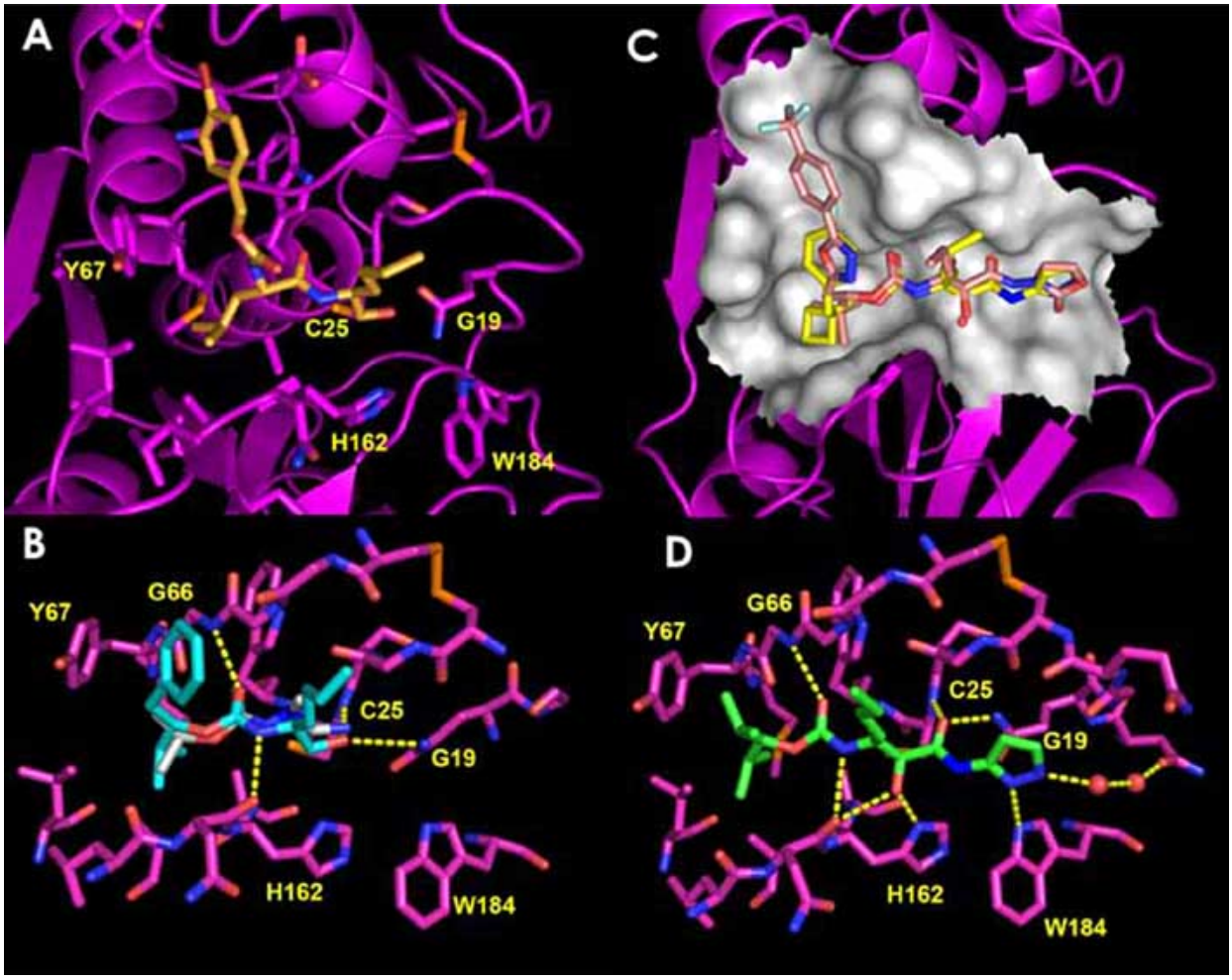

Fig. (1). **A**. Active site of the X-ray co-crystal structure of a *para*-bromo-derivative of calpeptin **1** bound to Cathepsin K. The cathepsin K carbons are colored magenta with inhibitor carbons colored orange. **B**. Active site of the X-ray co-crystal structure of aldehyde **53** and t-BuO(C=O)NHN(Me)CN bound to Cathepsin K. The cathepsin K carbons are colored magenta with the aldehyde carbons colored cyan and the cyanamide carbons colored white. The hydrogen bonds are depicted as yellow dashed lines. **C**. Active site of the X-ray co-crystal structure of ketoamide **234** and ketoamide **307** bound to Cathepsin K. The cathepsin K carbons are colored magenta with the ketoamide **234** carbons colored yellow and the ketoamide **307** carbons colored pink. The semi-transparent white surface represents the molecular surface. **D**. Active site of the X-ray co-crystal structure of ketoamide **169** bound to Cathepsin K. The cathepsin K carbons are colored magenta with the ketoamide carbons colored green. The hydrogen bonds are depicted as yellow dashed lines. This figure was generated using PYMOL version 0.93.

inhibitors with good pharmacokinetic properties and moderate selectivity. The ketoamide-based inhibitors attenuated bone resorption in relevant animal models of osteoporosis. Further improvements in selectivity in this series were precluded by strategic decisions at the merger of GlaxoWellcome and SmithKline Beecham terminating the GlaxoWellcome cathepsin K project. Nevertheless, these efforts demonstrated the viability of ketoamide-based inhibitors as potential drugs for the treatment of osteoporosis. With at least GlaxoSmithKline [156], Merck [199], and Novartis [155] conducting clinical trials, and Novartis reporting reductions in CTX in postmenopausal women, the future for cathepsin K inhibitors looks bright.

ACKNOWLEDGEMENTS

The authors would like to thank Aaron B. Miller for generation of the pictures of the cathepsin K/inhibitor X-ray co-crystal structures in (Fig. **1**).

REFERENCES

[1] Bilezikian, J. P.; Raisz, L. G.; Rodan, G. A.; Editors *Principles of Bone Biology*; Academic Press: San Diego, CA, **1996**.

[2] Marcus, R.; Feldman, D.; Kelsey, J.; Editors *Osteoporosis*; Academic Press: San Diego, CA, **1996**.

[3] Smith, E. P.; Boyd, J.; Frank, G. R.; Takahashi, H.; Cohen, R. M.; Specker, B.; Williams, T. C.; Lubahn, D. B.; Korach, K. S. Estrogen resistance caused by a mutation in the estrogen-receptor gene in a man. *New England Journal of Medecine* **1994**, *331*, 1056-1061.

[4] Taxel, P.; Kennedy, D. G.; Fall, P. M.; Willard, A. K.; Clive, J. M.; Raisz, L. G. The effect of aromatase inhibition on sex steroids, gonadotropins, and markers of bone turnover in older men. *Journal of Clinical Endocrinology Metabolism* **2001**, *86*, 2869-2874.

[5] Hofbauer, L. C.; Khosla, S.; Dunstan, C. R.; Lacey, D. L.; Spelsberg, T. C.; Riggs, B. L. Estrogen stimulates gene expression and protein production of osteoprotegerin in human osteoblastic cells. *Endocrinol.* **1999**, *140*, 4367-4370.

[6] Eghbali-Fatourechi, G.; Khosla, S.; Sanyal, A.; Boyle, W. J.; Lacey, D. L.; Riggs, B. L. Role of RANK ligand in mediating increased bone resorption in early postmenopausal women. *Journal of Clinical Investigation* **2003**, *111*, 1221-1230.

[7] Hughes, D. E.; Dai, A.; Tiffee, J. C.; Li, H. H.; Mundy, G. R.; Boyce, B. F. Estrogen promotes apoptosis of murine osteoclasts mediated by TGF-b. *Nature Medicine (New York)* **1996**, *2*, 1132-1136.

[8] Kousteni, S.; Bellido, T.; Plotkin, L. I.; O'Brien, C. A.; Bodenner, D. L.; Han, L.; Han, K.; DiGregorio, G. B.; Katzenellenbogen, J. A.; Katzenellenbogen, B. S.; Roberson, P. K.; Weinstein, R. S.; Jilka, R. L.; Manolagas, S. C. Nongenotropic, sex-nonspecific signaling through the estrogen or androgen receptors: dissociation from transcriptional activity. *Cell (Cambridge, Massachusetts)* **2001**, *104*, 719-730.

[9] Ke, H. Z.; Qi, H.; Chidsey-Frink, K. L.; Crawford, D. T.; Thompson, D. D. Lasofoxifene (CP-336,156) protects against the age-related changes in bone mass, bone strength, and total serum cholesterol in intact aged male rats. *Journal of Bone and Mineral Research* **2001**, *16*, 765-773.

[10] Fitzpatrick, L. A. Clinical trials of estrogen and SERMs on bone markers, bone mineral density, and fractures. *Osteoporosis* **2003**, 331-347.

[11] Sutherland, M. S. K.; Lipps, S. G.; Patnaik, N.; Gayo-Fung, L. M.; Khammungkune, S.; Xie, W.; Brady, H. A.; Barbosa, M. S.; Anderson, D. W.; Stein, B. SP500263, a novel SERM, blocks osteoclastogenesis in a human bone cell model: role of IL-6 and GM-CSF. *Cytokine* **2003**, *23*, 1-14.

[12] Tiitinen, A.; Nikander, E.; Hietanen, P.; Metsae-Heikkila, M.; Ylikorkala, O. Changes in bone mineral density during and after 3 years' use of tamoxifen or toremifene. *Maturitas* **2004**, *48*, 321-327.

[13] Petersen, N. M.; Briggs, A. L. Selective estrogen receptor modulators. *Clinical Reviews in Bone and Mineral Metabolism* **2005**, *3*, 19-30.

[14] Rogers, M. J. New insights into the molecular mechanisms of action of bisphosphonates. *Current Pharmaceutical Design* **2003**, *9*, 2643-2658.

[15] Benford, H. L.; McGowan, N. W. A.; Helfrich, M. H.; Nuttall, M. E.; Rogers, M. J. Visualization of bisphosphonate-induced caspase-3 activity in apoptotic osteoclasts *in vitro*. *Bone (New York, NY, United States)* **2001**, *28*, 465-473.

[16] Rogers, M. J.; Brown, R. J.; Hodkin, V.; Blackburn, G. M.; Russell, R. G. G.; Watts, D. J. Bisphosphonates are incorporated into adenine nucleotides by human aminoacyl-tRNA synthetase enzymes. *Biochemical and Biophysical Research Communications* **1996**, *224*, 863-869.

[17] Fisher, J. E.; Rogers, M. J.; Halasy, J. M.; Luckman, S. P.; Hughes, D. E.; Masarachia, P. J.; Wesolowski, G.; Russell, R. G. G.; Rodan, G. A.; Reszka, A. A. Alendronate mechanism of action: geranylgeraniol, an intermediate in the mevalonate pathway, prevents inhibition of osteoclast formation, bone resorption, and kinase activation *in vitro*. *Proceedings of the National Academy of Sciences of the United States of America* **1999**, *96*, 133-138.

[18] Staal, A.; Frith, J. C.; French, M. H.; Swartz, J.; Gungor, T.; Harrity, T. W.; Tamasi, J.; Rogers, M. J.; Feyen, J. H. M. The ability of statins to inhibit bone resorption is directly related to their inhibitory effect on HMG-CoA reductase activity. *Journal of Bone and Mineral Research* **2003**, *18*, 88-96.

[19] Kallio, D. M.; Garant, P. R.; Minkin, C. Ultrastructural effects of calcitonin on osteoclasts in tissue culture. *Journal of Ultrastructure Research* **1972**, *39*, 205-216.

[20] Holtrop, M. E.; Raisz, L. G.; Simmons, H. A. Effects of parathyroid hormone, colchicine, and calcitonin on the ultrastructure and the activity of osteoclasts in organ culture. *Journal of Cell Biology* **1974**, *60*, 346-355.

[21] Nicholson, G. C.; Moseley, J. M.; Sexton, P. M.; Mendelsohn, F. A. O.; Martin, T. J. Abundant calcitonin receptors in isolated rat osteoclasts. Biochemical and autoradiographic characterization. *Journal of Clinical Investigation* **1986**, *78*, 355-360.

[22] Dursun, N.; Dursun, E.; Yalcin, S. Comparison of alendronate, calcitonin and calcium treatments in postmenopausal osteoporosis. *International Journal of Clinical Practice* **2001**, *55*, 505-509.

[23] Cranney, A.; Tugwell, P.; Zytaruk, N.; Robinson, V.; Weaver, B.; Shea, B.; Wells, G.; Adachi, J.; Waldegger, L.; Guyatt, G. Meta-analysis of calcitonin for the treatment of postmenopausal osteoporosis. *Endocrine Reviews* **2002**, *23*, 540-551.

[24] Teitelbaum, S. L. Osteoclasts, integrins, and osteoporosis. *Journal of Bone and Mineral Metabolism* **2000**, *18*, 344-349.

[25] McHugh, K. P.; Hodivala-Dilke, K.; Zheng, M.-H.; Namba, N.; Lam, J.; Novack, D.; Feng, X.; Ross, F. P.; Hynes, R. O.; Teitelbaum, S. L. Mice lacking b3 integrins are osteosclerotic because of dysfunctional osteoclasts. *Journal of Clinical Investigation* **2000**, *105*, 433-440.

[26] Lane, N. E.; Yao, W.; Nakamura, M. C.; Humphrey, M. B.; Kimmel, D.; Huang, X.; Sheppard, D.; Ross, F. P.; Teitelbaum, S. L. Mice lacking the integrin b5 subunit have accelerated osteoclast maturation and increased activity in the estrogen-deficient state. *Journal of Bone and Mineral Research* **2005**, *20*, 58-66.

[27] Hartman, G. D.; Duggan, M. E. avb3 integrin antagonists as inhibitors of bone resorption. *Expert Opinion on Investigational Drugs* **2000**, *9*, 1281-1291.

[28] Murphy, M. G.; Cerchio, K.; Stoch, S. A.; Gottesdiener, K.; Wu, M.; Recker, R. Effect of L-000845704, an avb3 integrin antagonist, on markers of bone turnover and bone mineral density in postmenopausal osteoporotic women. *Journal of Clinical Endocrinology and Metabolism* **2005**, *90*, 2022-2028.

[29] Murphy, M.; Cerchio, K.; Stoch, S.; Gottesdiener, K.; Wu, M.; Recker, R. Effects of MRL123, an orally administered αvβ3 integrin antagonist, on markers of bone turnover and bone mineral density in postmenopausal osteoporotic women. *J. Bone Miner. Res.* **2004**, *19*, S99.

[30] Kornak, U.; Kasper, D.; Bosl, M. R.; Kaiser, E.; Schweizer, M.; Schulz, A.; Friedrich, W.; Delling, G.; Jentsch, T. J. Loss of the ClC-7 chloride channel leads to osteopetrosis in mice and man. *Cell* **2001**, *104*, 205-215.

[31] Schaller, S.; Henriksen, K.; Sveigaard, C.; Heegaard, A.-M.; Helix, N.; Stahlhut, M.; Ovejero, M. C.; Johansen, J. V.; Solberg, H.; Andersen, T. L.; Hougaard, D.; Berryman, M.; Shiodt, C. B.; Sorensen, B. H.; Lichtenberg, J.; Christophersen, P.; Foged, N. T.; Delaisse, J.-M.; Engsig, M. T.; Karsdal, M. A. The chloride channel inhibitor N53736 prevents bone resorption in ovariectomized rats without changing bone formation. *Journal of Bone and Mineral Research* **2004**, *19*, 1144-1153.

[32] Blair, H. C.; Teitelbaum, S. L.; Ghiselli, R.; Gluck, S. Osteoclastic bone resorption by a polarized vacuolar proton pump. *Science (Washington, DC, United States)* **1989**, *245*, 855-857.

[33] Farina, C.; Gagliardi, S. Selective inhibition of osteoclast vacuolar H+-ATPase. *Current Pharmaceutical Design* **2002**, *8*, 2033-2048.

[34] Karsdal, M. A.; Henriksen, K.; Sorensen, M. G.; Gram, J.; Schaller, S.; Dziegiel, M. H.; Heegaard, A.-M.; Christophersen, P.; Martin, T. J.; Christiansen, C.; Bollerslev, J. Acidification of the osteoclastic resorption compartment provides insight into the coupling of bone formation to bone resorption. *American Journal of Pathology* **2005**, *166*, 467-476.

[35] Sly, W. S.; Hewett-Emmett, D.; Whyte, M. P.; Yu, Y. S.; Tashian, R. E. Carbonic anhydrase II deficiency identified as the primary defect in the autosomal recessive syndrome of osteopetrosis with renal tubular acidosis and cerebral calcification. *Proceedings of the National Academy of Sciences of the United States of America* **1983**, *80*, 2752-2756.

[36] Ohba, Y.; Ohba, T.; Sumitani, K.; Tagami-Kondoh, K.; Hiura, K.; Miki, Y.; Kakegawa, H.; Katunuma, N.; Takano-Yamamoto, T. Inhibitory mechanisms of H+-ATPase inhibitor bafilomycin A1 and carbonic anhydrase II inhibitor acetazolamide on experimental bone resorption. *FEBS Letters* **1996**, *387*, 175-178.

[37] Lehenkari, P.; Hentunen, T. A.; Laitala-Leinonen, T.; Tuukkanen, J.; Vaananen, H. K. Carbonic anhydrase II plays a major role in osteoclast differentiation and bone resorption by effecting the steady state intracellular pH and Ca2+. *Experimental Cell Research* **1998**, *242*, 128-137.

[38] Gay, C. V.; Mueller, W. J. Carbonic anhydrase and osteoclasts. Localization by labeled inhibitor autoradiography. *Science (Washington, DC, United States)* **1974**, *183*, 432-434.

[39] Rousselle, A. V.; Heymann, D. Osteoclastic acidification pathways during bone resorption. *Bone (New York, NY, United States)* **2002**, *30*, 533-540.

[40] Hall, T. J.; Schaeublin, M.; Chambers, T. J. Sodium/hydrogen ion antiporter activity is essential for the induction, but not the maintenance of osteoclastic bone resorption and cytoplasmic spreading. *Biochemical and Biophysical Research Communications* **1992**, *188*, 1097-1103.

[41] Keeling, D. J.; Herslof, M.; Mattsson, J. P.; Ryberg, B. Tissue-selective inhibition of vacuolar acid pumps. *Acta Physiologica Scandinavica, Supplementum* **1998**, *163*, 195-201.

[42] Kasper, D.; Planells-Cases, R.; Fuhrmann, J. C.; Scheel, O.; Zeitz, O.; Ruether, K.; Schmitt, A.; Poet, M.; Steinfeld, R.; Schweizer, M.; Kornak, U.; Jentsch, T. J. Loss of the chloride channel ClC-7 leads to lysosomal storage disease and neurodegeneration. *EMBO Journal* **2005**, *24*, 1079-1091.

[43] Visentin, L.; Dodds, R. A.; Valente, M.; Misiano, P.; Bradbeer, J. N.; Oneta, S.; Liang, X.; Gowen, M.; Farina, C. A selective inhibitor of the osteoclastic V-H+-ATPase prevents bone loss in both thyroparathyroidectomized and ovariectomized rats. *Journal of Clinical Investigation* **2000**, *106*, 309-318.

[44] Niikura, K.; Takano, M.; Sawada, M. A novel inhibitor of vacuolar ATPase, FR167356, which can discriminate between osteoclast vacuolar ATPase and lysosomal vacuolar ATPase. *British Journal of Pharmacology* **2004**, *142*, 558-566.

[45] Jilka, R. L.; Weinstein, R. S.; Bellido, T.; Roberson, P.; Parfitt, A. M.; Manolagas, S. C. Increased bone formation by prevention of osteoblast apoptosis with parathyroid hormone. *Journal of Clinical Investigation* **1999**, *104*, 439-446.

[46] Rittmaster, R. S.; Bolognese, M.; Ettinger, M. P.; Hanley, D. A.; Hodsman, A. B.; Kendler, D. L.; Rosen, C. J. Enhancement of bone mass in osteoporotic women with parathyroid hormone followed by alendronate. *Journal of Clinical Endocrinology and Metabolism* **2000**, *85*, 2129-2134.

[47] Nemeth, E. F.; Delmar, E. G.; Heaton, W. L.; Miller, M. A.; Lambert, L. D.; Conklin, R. L.; Gowen, M.; Gleason, J. G.; Bhatnagar, P. K.; Fox, J. Calcilytic compounds: potent and selective Ca2+ receptor antagonists that stimulate secretion of parathyroid hormone. *Journal of Pharmacology and Experimental Therapeutics* **2001**, *299*, 323-331.

[48] Arey, B. J.; Seethala, R.; Ma, Z.; Fura, A.; Morin, J.; Swartz, J.; Vyas, V.; Yang, W.; Dickson, J. K. Jr.; Feyen, J. H. M. A novel calcium-sensing receptor antagonist transiently stimulates parathyroid hormone secretion *in vivo*. *Endocrinology* **2005**, *146*, 2015-2022.

[49] Pederson, L.; Kremer, M.; Judd, J.; Pascoe, D.; Spelsberg, T. C.; Riggs, B. L.; Oursler, M. J. Androgens regulate bone resorption activity of isolated osteoclasts *in vitro*. *Proceedings of the National Academy of Sciences of the United States of America* **1999**, *96*, 505-510.

[50] Chen, J. R.; Kousteni, S.; Bellido, T.; Han, L.; DiGregorio, G. B.; Jilka, R. L.; Manolagas, S. C. Gender-independent induction of murine osteoclast apoptosis *in vitro* by either estrogens or nonaromatizable androgens. *J. Bone Miner. Res.* **2001**, S159.

[51] Dalton, J. T.; Mukherjee, A.; Zhu, Z.; Kirkovsky, L.; Miller, D. D. Discovery of nonsteroidal androgens. *Biochemical and Biophysical Research Communications* **1998**, *244*, 1-4.

[52] Kirkovsky, L.; Mukherjee, A.; Yin, D.; Dalton, J. T.; Miller, D. D. Chiral Nonsteroidal Affinity Ligands for the Androgen Receptor. 1. Bicalutamide Analogues Bearing Electrophilic Groups in the B Aromatic Ring. *Journal of Medicinal Chemistry* **2000**, *43*, 581-590.

[53] He, Y.; Yin, D.; Perera, M.; Kirkovsky, L.; Stourman, N.; Li, W.; Dalton, J. T.; Miller, D. D. Novel nonsteroidal ligands with high binding affinity and potent functional activity for the androgen receptor. *European Journal of Medicinal Chemistry* **2002**, *37*, 619-634.

[54] Rosen, J.; Negro-Vilar, A. Novel, non-steroidal, selective androgen receptor modulators (SARMs) with anabolic activity in bone and muscle and improved safety profile. *Journal of Musculoskeletal & Neuronal Interactions* **2002**, *2*, 222-224.

[55] Winkler, D. G.; Sutherland, M. K.; Geoghegan, J. C.; Yu, C.; Hayes, T.; Skonier, J. E.; Shpektor, D.; Jonas, M.; Kovacevich, B. R.; Staehling-Hampton, K.; Appleby, M.; Brunkow, M. E.; Latham, J. A. Osteocyte control of bone formation *via* sclerostin, a novel BMP antagonist. *EMBO Journal* **2003**, *22*, 6267-6276.

[56] Van Bezooijen, R. L.; Roelen, B. A. J.; Visser, A.; Van der Wee-Pals, L.; De Wilt, E.; Karperien, M.; Hamersma, H.; Papapoulos, S. E.; ten Dijke, P.; Loewik, C. W. G. M. Sclerostin is an osteocyte-expressed negative regulator of bone formation, but not a classical BMP antagonist. *Journal of Experimental Medicine* **2004**, *199*, 805-814.

[57] Yanagita, M. BMP antagonists: Their roles in development and involvement in pathophysiology. *Cytokine & Growth Factor Reviews* **2005**, *16*, 309-317.

[58] Garrett, I. R.; Chen, D.; Gutierrez, G.; Zhao, M.; Escobedo, A.; Rossini, G.; Harris, S. E.; Gallwitz, W.; Kim, K. B.; Hu, S.; Crews, C. M.; Mundy, G. R. Selective inhibitors of the osteoblast proteasome stimulate bone formation *in vivo* and *in vitro*. *Journal of Clinical Investigation* **2003**, *111*, 1771-1782.

[59] Marie, P. J.; Hott, M.; Modrowski, D.; De Pollak, C.; Guillemain, J.; Deloffre, P.; Tsouderos, Y. An uncoupling agent containing strontium prevents bone loss by depressing bone resorption and maintaining bone formation in estrogen-deficient rats. *Journal of Bone and Mineral Research* **1993**, *8*, 607-615.

[60] Marie, P. J.; Ammann, P.; Boivin, G.; Rey, C. Mechanisms of action and therapeutic potential of strontium in bone. *Calcified Tissue International* **2001**, *69*, 121-129.

[61] Meunier, P. J.; Slosman, D. O.; Delmas, P. D.; Sebert, J. L.; Brandi, M. L.; Albanese, C.; Lorenc, R.; Pors-Nielsen, S.; De Vernejoul, M. C.; Roces, A.; Reginster, J. Y. Strontium ranelate: Dose-dependent effects in established postmenopausal vertebral osteoporosis-A 2-year randomized placebo controlled trial. *Journal of Clinical Endocrinology and Metabolism* **2002**, *87*, 2060-2066.

[62] Reginster, J. Y.; Seeman, E.; De Vernejoul, M. C.; Adami, S.; Compston, J.; Phenekos, C.; Devogelaer, J. P.; Curiel, M. D.; Sawicki, A.; Goemaere, S.; Sorensen, O. H.; Felsenberg, D.; Meunier, P. J. Strontium ranelate reduces the risk of nonvertebral fractures in postmenopausal women with osteoporosis: Treatment of peripheral osteoporosis (TROPOS) study. *Journal of Clinical Endocrinology and Metabolism* **2005**, *90*, 2816-2822.

[63] Stains, J. P.; Civitelli, R. Cell-to-cell interactions in bone. *Biochemical and Biophysical Research Communications* **2005**, *328*, 721-727.

[64] Cheng, S.-L.; Shin, C. S.; Towler, D. A.; Civitelli, R. A dominant negative cadherin inhibits osteoblast differentiation. *Journal of Bone and Mineral Research* **2000**, *15*, 2362-2370.

[65] Ferrari, S. L.; Traianedes, K.; Thorne, M.; Lafage-Proust, M.-H.; Genever, P.; Cecchini, M. G.; Behar, V.; Bisello, A.; Chorev, M.; Rosenblatt, M.; Suva, L. J. A role for N-cadherin in the development of the differentiated osteoblastic phenotype. *Journal of Bone and Mineral Research* **2000**, *15*, 198-208.

[66] Hay, E.; Lemonnier, J.; Modrowski, D.; Lomri, A.; Lasmoles, F.; Marie, P. J. N- and E-cadherin mediate early human calvaria osteoblast differentiation promoted by bone morphogenetic protein-2. *Journal of Cellular Physiology* **2000**, *183*, 117-128.

[67] Vander Molen, M. A.; Rubin, C. T.; McLeod, K. J.; McCauley, L. K.; Donahue, H. J. Gap junctional intercellular communication contributes to hormonal responsiveness in osteoblastic networks. *Journal of Biological Chemistry* **1996**, *271*, 12165-12171.

[68] Lecanda, F.; Towler, D. A.; Ziambaras, K.; Cheng, S.-L.; Koval, M.; Steinberg, T. H.; Civitelli, R. Gap junctional communication modulates gene expression in osteoblastic cells. *Molecular Biology of the Cell* **1998**, *9*, 2249-2258.

[69] Schiller, P. C.; D'Ippolito, G.; Balkan, W.; Roos, B. A.; Howard, G. A. Gap-junctional communication is required for the maturation process of osteoblastic cells in culture. *Bone (New York, NY, United States)* **2001**, *28*, 362-369.

[70] Dougall, W. C.; Glaccum, M.; Charrier, K.; Rohrbach, K.; Brasel, K.; De Smedt, T.; Daro, E.; Smith, J.; Tometsko, M. E.; Maliszewski, C. R.; Armstrong, A.; Shen, V.; Bain, S.; Cosman, D.; Anderson, D.; Morrissey, P. J.; Peschon, J. J.; Schuh, J. RANK is essential for osteoclast and lymph node development. *Genes & Development* **1999**, *13*, 2412-2424.

[71] Kong, Y.-Y.; Yoshida, H.; Sarosi, I.; Tan, H.-L.; Timms, E.; Capparelli, C.; Morony, S.; Oliveira-Dos-Santos, A. J.; Van, G.; Itie, A.; Khoo, W.; Wakeham, A.; Dunstan, C. R.; Lacey, D. L.; Mak, T. W.; Boyle, W. J.; Penninger, J. M. OPGL is a key regulator of osteoclastogenesis, lymphocyte development and lymph-node organogenesis. *Nature (London)* **1999**, *397*, 315-323.

[72] Bekker, P. J.; Holloway, D. L.; Rasmussen, A. S.; Murphy, R.; Martin, S. W.; Leese, P. T.; Holmes, G. B.; Dunstan, C. R.;

DePaoli, A. M. A single-dose placebo-controlled study of AMG 162, a fully human monoclonal antibody to RANKL, in postmenopausal women. *Journal of Bone and Mineral Research* **2004**, *19*, 1059-1066.

[73] McClung, M. R.; Lewiecki, E. M.; Bolognese, M. A.; Woodson, G.; Moffett, A.; Peacock, M.; Miller, P. D.; Lederman, S.; Chestnut, C. H.; Murphy, R. AMG 162 increases bone mineral density (BMD) within 1 month in postmenopausal women with low BMD. *J. Bone Miner. Res.* **2004**, *19*, S20.

[74] Arai, F.; Miyamoto, T.; Ohneda, O.; Inada, T.; Sudo, T.; Brasel, K.; Miyata, T.; Anderson, D. M.; Suda, T. Commitment and differentiation of osteoclast precursor cells by the sequential expression of c-Fms and receptor activator of nuclear factor kB (RANK) receptors. *Journal of Experimental Medicine* **1999**, *190*, 1741-1754.

[75] Ariyoshi, W.; Takahashi, T.; Kanno, T.; Ichimiya, H.; Takano, H.; Koseki, T.; Nishihara, T. Mechanisms Involved in Enhancement of Osteoclast Formation and Function by Low Molecular Weight Hyaluronic Acid. *Journal of Biological Chemistry* **2005**, *280*, 18967-18972.

[76] Tondravi, M. M.; McKercher, S. R.; Anderson, K.; Erdmann, J. M.; Quiroz, M.; Maki, R.; Teitelbaum, S. L. Osteopetrosis in mice lacking hematopoietic transcription factor PU.1. *Nature (London)* **1997**, *386*, 81-84.

[77] Udagawa, N.; Horwood, N. J.; Elliott, J.; Mackay, A.; Owens, J.; Okamura, H.; Kurimoto, M.; Chambers, T. J.; Martin, T. J.; Gillespie, M. T. Interleukin-18 (interferon-g-inducing factor) is produced by osteoblasts and acts *via* granulocyte/macrophage colony-stimulating factor and not *via* interferon-g to inhibit osteoclast formation. *Journal of Experimental Medicine* **1997**, *185*, 1005-1012.

[78] Miyamoto, T.; Ohneda, O.; Arai, F.; Iwamoto, K.; Okada, S.; Takagi, K.; Anderson, D. M.; Suda, T. Bifurcation of osteoclasts and dendritic cells from common progenitors. *Blood* **2001**, *98*, 2544-2554.

[79] Horowitz, M. C.; Lorenzo, J. A. In *Principles of Bone Biology (2nd Edition)* 2002; Vol. 2, p 961-977.

[80] Mirosavljevic, D.; Quinn, J. M. W.; Elliott, J.; Horwood, N. J.; Martin, T. J.; Gillespie, M. T. T-cells mediate an inhibitory effect of interleukin-4 on osteoclastogenesis. *Journal of Bone and Mineral Research* **2003**, *18*, 984-993.

[81] Hodge, J. M.; Kirkland, M. A.; Aitken, C. J.; Waugh, C. M.; Myers, D. E.; Lopez, C. M.; Adams, B. E.; Nicholson, G. C. Osteoclastic potential of human CFU-GM: biphasic effect of GM-CSF. *Journal of Bone and Mineral Research* **2004**, *19*, 190-199.

[82] Kamolmatyakul, S.; Chen, W.; Yang, S.; Abe, Y.; Moroi, R.; Ashique, A. M.; Li, Y. P. IL-1a stimulates cathepsin K expression in osteoclasts *via* the tyrosine kinase-NF-kB pathway. *Journal of Dental Research* **2004**, *83*, 791-796.

[83] Quinn, J. M. W.; Gillespie, M. T. Modulation of osteoclast formation. *Biochemical and Biophysical Research Communications* **2005**, *328*, 739-745.

[84] Simonet, W. S.; Lacey, D. L.; Dunstan, C. R.; Kelley, M.; Chang, M. S.; Luthy, R.; Nguyen, H. C.; Wooden, S.; Bennett, L.; Boone, T.; Shimamoto, G.; DeRose, M.; Elliott, R.; Colombero, A.; Tan, H. L.; Trail, G.; Sullivan, J.; Davy, E.; Bucay, N.; Renshaw-Gregg, L.; Hughes, T. M.; Hill, D.; Pattison, W.; Campbell, P.; Sander, S.; Van, G.; Tarpley, J.; Derby, P.; Lee, R.; Boyle, W. J. Osteoprotegerin: a novel secreted protein involved in the regulation of bone density. *Cell (Cambridge, Massachusetts)* **1997**, *89*, 309-319.

[85] Lacey, D. L.; Timms, E.; Tan, H. L.; Kelley, M. J.; Dunstan, C. R.; Burgess, T.; Elliott, R.; Colombero, A.; Elliott, G.; Scully, S.; Hsu, H.; Sullivan, J.; Hawkins, N.; Davy, E.; Capparelli, C.; Eli, A.; Qian, Y. X.; Kaufman, S.; Sarosi, I.; Shalhoub, V.; Senaldi, G.; Guo, J.; Delaney, J.; Boyle, W. J. Osteoprotegerin ligand is a cytokine that regulates osteoclast differentiation and activation. *Cell (Cambridge, Massachusetts)* **1998**, *93*, 165-176.

[86] Yasuda, H.; Shima, N.; Nakagawa, N.; Yamaguchi, K.; Kinosaki, M.; Mochizuki, S.-I.; Tomoyasu, A.; Yano, K.; Goto, M.; Murakami, A.; Tsuda, E.; Morinaga, T.; Higashio, K.; Udagawa, N.; Takahashi, N.; Suda, T. Osteoclast differentiation factor is a ligand for osteoprotegerin/osteoclastogenesis-inhibitory factor and is identical to TRANCE/RANKL. *Proceedings of the National Academy of Sciences of the United States of America* **1998**, *95*, 3597-3602.

[87] Mizuno, A.; Amizuka, N.; Irie, K.; Murakami, A.; Fujise, N.; Kanno, T.; Sato, Y.; Nakagawa, N.; Yasuda, H.; Mochizuki, S.-i.; Gomibuchi, T.; Yano, K.; Shima, N.; Washida, N.; Tsuda, E.; Morinaga, T.; Higashio, K.; Ozawa, H. Severe osteoporosis in mice lacking osteoclastogenesis inhibitory factor/osteoprotegerin. *Biochemical and Biophysical Research Communications* **1998**, *247*, 610-615.

[88] Takai, H.; Kanematsu, M.; Yano, K.; Tsuda, E.; Higashio, K.; Ikeda, K.; Watanabe, K.; Yamada, Y. Transforming growth factor-b stimulates the production of osteoprotegerin/osteoclastogenesis inhibitory factor by bone marrow stromal cells. *Journal of Biological Chemistry* **1998**, *273*, 27091-27096.

[89] Quinn, J. M. W.; Itoh, K.; Udagawa, N.; Hausler, K.; Yasuda, H.; Shima, N.; Mizuno, A.; Higashio, K.; Takahashi, N.; Suda, T.; Martin, T. J.; Gillespie, M. T. Transforming growth factor b affects osteoclast differentiation *via* direct and indirect actions. *Journal of Bone and Mineral Research* **2001**, *16*, 1787-1794.

[90] Minkin, C. Bone acid phosphatase: tartrate-resistant acid phosphatase as a marker of osteoclast function. *Calcified Tissue International* **1982**, *34*, 285-290.

[91] Funhoff, E. G.; Ljusberg, J.; Wang, Y.; Andersson, G.; Averill, B. A. Mutational Analysis of the Interaction between Active Site Residues and the Loop Region in Mammalian Purple Acid Phosphatases. *Biochemistry* **2001**, *40*, 11614-11622.

[92] Ljusberg, J.; Wang, Y.; Lang, P.; Norgard, M.; Dodds, R.; Hultenby, K.; Ek-Rylander, B.; Andersson, G. Proteolytic excision of a repressive loop domain in tartrate-resistant acid phosphatase by cathepsin K in osteoclasts. *Journal of Biological Chemistry* **2005**, *280*, 28370-28381.

[93] Hayman, A. R.; Jones, S. J.; Boyde, A.; Foster, D.; Colledge, W. H.; Carlton, M. B.; Evans, M. J.; Cox, T. M. Mice lacking tartrate-resistant acid phosphatase (Acp 5) have disrupted endochondral ossification and mild osteopetrosis. *Development (Cambridge, United Kingdom)* **1996**, *122*, 3151-3162.

[94] Hollberg, K.; Hultenby, K.; Hayman, A. R.; Cox, T. M.; Andersson, G. Osteoclasts from Mice Deficient in Tartrate-Resistant Acid Phosphatase Have Altered Ruffled Borders and Disturbed Intracellular Vesicular Transport. *Experimental Cell Research* **2002**, *279*, 227-238.

[95] Angel, N. Z.; Walsh, N.; Forwood, M. R.; Ostrowski, M. C.; Cassady, A. I.; Hume, D. A. Transgenic mice over-expressing tartrate-resistant acid phosphatase exhibit an increased rate of bone turnover. *Journal of Bone and Mineral Research* **2000**, *15*, 103-110.

[96] Grigoriadis, A. E.; Wang, Z.-Q.; Cecchini, M. G.; Hofstetter, W.; Felix, R.; Fleisch, H. A.; Wagner, E. F. c-Fos: A key regulator of osteoclast-macrophage lineage determination and bone remodeling. *Science (Washington, D. C.)* **1994**, *266*, 443-448.

[97] Jimi, E.; Aoki, K.; Saito, H.; D'Acquisto, F.; May, M. J.; Nakamura, I.; Sudo, T.; Kojima, T.; Okamoto, F.; Fukushima, H.; Okabe, K.; Ohya, K.; Ghosh, S. Selective inhibition of NF-kB blocks osteoclastogenesis and prevents inflammatory bone destruction *in vivo*. *Nature Medicine (New York, NY, United States)* **2004**, *10*, 617-624.

[98] May, M. J.; D'Acquisto, F.; Madge, L. A.; Glockner, J.; Pober, J. S.; Ghosho, S. Selective inhibition of NF-kb activation by a peptide that blocks the interaction of NEMO with the IkB kinase complex. *Science (Washington, D. C.)* **2000**, *289*, 1550-1554.

[99] Soriano, P.; Montgomery, C.; Geske, R.; Bradley, A. Targeted disruption of the c-src proto-oncogene leads to osteopetrosis in mice. *Cell (Cambridge, MA, United States)* **1991**, *64*, 693-702.

[100] Lowe, C.; Yoneda, T.; Boyce, B. F.; Chen, H.; Mundy, G. R.; Soriano, P. Osteopetrosis in Src-deficient mice is due to an autonomous defect of osteoclasts. *Proceedings of the National Academy of Sciences of the United States of America* **1993**, *90*, 4485-4489.

[101] Nakamura, I.; Jimi, E.; Duong, L. T.; Sasaki, T.; Takahashi, N.; Rodan, G. A.; Suda, T. Tyrosine phosphorylation of p130Cas is involved in actin organization in osteoclasts. *Journal of Biological Chemistry* **1998**, *273*, 11144-11149.

[102] Lakkakorpi, P. T.; Nakamura, I.; Nagy, R. M.; Parsons, J. T.; Rodan, G. A.; Duong, L. T. Stable association of PYK2 and p130Cas in osteoclasts and their co-localization in the sealing zone. *Journal of Biological Chemistry* **1999**, *274*, 4900-4907.

[103] Metcalf, C. A., III; Van Schravendijk, M. R.; Dalgarno, D. C.; Sawyer, T. K. Targeting protein kinases for bone disease: discovery

and development of Src inhibitors. *Current Pharmaceutical Design* **2002**, *8*, 2049-2075.

[104] Marzia, M.; Sims, N. A.; Voit, S.; Migliaccio, S.; Taranta, A.; Bernardini, S.; Faraggiana, T.; Yoneda, T.; Mundy, G. R.; Boyce, B. F.; Baron, R.; Teti, A. Decreased c-Src expression enhances osteoblast differentiation and bone formation. *Journal of Cell Biology* **2000**, *151*, 311-320.

[105] Boyce, B. F.; Yoneda, T.; Lowe, C.; Soriano, P.; Mundy, G. R. Requirement of pp60c-src expression for osteoclasts to form ruffled borders and resorb bone in mice. *Journal of Clinical Investigation* **1992**, *90*, 1622-1627.

[106] Lakkakorpi, P. T.; Nakamura, I.; Young, M.; Lipfert, L.; Rodan, G. A.; Duong, L. T. Abnormal localization and hyperclustering of avb3 integrins and associated proteins in Src-deficient or tyrphostin A9-treated osteoclasts. *Journal of Cell Science* **2001**, *114*, 149-160.

[107] Sanjay, A.; Houghton, A.; Neff, L.; DiDomenico, E.; Bardelay, C.; Antoine, E.; Levy, J.; Gailit, J.; Bowtell, D.; Horne, W. C.; Baron, R. Cbl associates with Pyk2 and Src to regulate Src kinase activity, avb3 integrin-mediated signaling, cell adhesion, and osteoclast motility. *Journal of Cell Biology* **2001**, *152*, 181-195.

[108] Asaba, H.; Sasaki, J. Wnt signaling and bone metabolism. *Clinical Calcium* **2005**, *15*, 813-818.

[109] Garnero, P.; Borel, O.; Byrjalsen, I.; Ferreras, M.; Drake, F. H.; McQueney, M. S.; Foged, N. T.; Delmas, P. D.; Delaisse, J.-M. The collagenolytic activity of cathepsin K is unique among mammalian proteinases. *Journal of Biological Chemistry* **1998**, *273*, 32347-32352.

[110] Li, Z.; Hou, W.-S.; Escalante-Torres, C. R.; Gelb, B. D.; Bromme, D. Collagenase activity of cathepsin K depends on complex formation with chondroitin sulfate. *Journal of Biological Chemistry* **2002**, *277*, 28669-28676.

[111] McQueney, M. S.; Amegadzie, B. Y.; D'Alessio, K.; Hanning, C. R.; McLaughlin, M. M.; McNulty, D.; Carr, S. A.; Ijames, C.; Kurdyla, J.; Jones, C. S. Autocatalytic activation of human cathepsin K. *Journal of Biological Chemistry* **1997**, *272*, 13955-13960.

[112] LaLonde, J. M.; Zhao, B.; Janson, C. A.; D'Alessio, K. J.; McQueney, M. S.; Orsini, M. J.; Debouck, C. M.; Smith, W. W. The crystal structure of human procathepsin K. *Biochemistry* **1999**, *38*, 862-869.

[113] Atley, L. M.; Mort, J. S.; Lalumiere, M.; Eyre, D. R. Proteolysis of human bone collagen by cathepsin K: characterization of the cleavage sites generating the cross-linked N-telopeptide neoepitope. *Bone (New York)* **2000**, *26*, 241-247.

[114] Morko, J.; Kiviranta, R.; Hurme, S.; Rantakokko, J.; Vuorio, E. Differential turnover of cortical and trabecular bone in transgenic mice overexpressing cathepsin K. *Bone (San Diego, CA, United States)* **2005**, *36*, 854-865.

[115] Tezuka, K.; Tezuka, Y.; Maejima, A.; Sato, T.; Nemoto, K.; Kamioka, H.; Hakeda, Y.; Kumegawa, M. Molecular cloning of a possible cysteine proteinase predominantly expressed in osteoclasts. *Journal of Biological Chemistry* **1994**, *269*, 1106-1109.

[116] Bromme, D.; Okamoto, K. Human cathepsin O2, a novel cysteine protease highly expressed in osteoclastomas and ovary molecular cloning, sequencing and tissue distribution. *Biological Chemistry Hoppe-Seyler* **1995**, *376*, 379-384.

[117] Inaoka, T.; Bilbe, G.; Ishibashi, O.; Tezuka, K.; Kumegawa, M.; Kokubo, T. Molecular cloning of human cDNA for cathepsin K: Novel cysteine proteinase predominantly expressed in bone. *Biochemical and Biophysical Research Communications* **1995**, *206*, 89-96.

[118] Drake, F. H.; Dodds, R. A.; James, I. E.; Connor, J. R.; Debouck, C.; Richardson, S.; Lee-Rykaczewski, E.; Coleman, L.; Rieman, D.; Barthlow, R.; Hastings, G.; Gowen, M. Cathepsin K, but not cathepsins B, L, or S, is abundantly expressed in human osteoclasts. *Journal of Biological Chemistry* **1996**, *271*, 12511-12516.

[119] Gelb, B. D.; Moissoglu, K.; Zhang, J.; Martignetti, J. A.; Bromme, D.; Desnick, R. J. Cathepsin K: isolation and characterization of the murine cDNA and genomic sequence, the homolog of the human pycnodysostosis gene. *Biochemical and Molecular Medicine* **1996**, *59*, 200-206.

[120] Gelb, B. D.; Shi, G.-P.; Chapman, H. A.; Desnick, R. J. Pycnodysostosis, a lysosomal disease caused by cathepsin K deficiency. *Science* **1996**, *273*, 1236-1238.

[121] Johnson, M. R.; Polymeropoulos, M. H.; Vos, H. L.; Ortiz de Luna, R. I.; Francomano, C. A. A nonsense mutation in the cathepsin K gene observed in a family with pycnodysostosis. *Genome Research* **1996**, *6*, 1050-1055.

[122] Motyckova, G.; Fisher, D. E. Pycnodysostosis: role and regulation of cathepsin K in osteoclast function and human disease. *Curr. Mol. Med.* **2002**, *2*, 407-421.

[123] Saftig, P.; Hunziker, E.; Wehmeyer, O.; Jones, S.; Boyde, A.; Rommerskirch, W.; Moritz, J. D.; Schu, P.; Von Figura, K. Impaired osteoclastic bone resorption leads to osteopetrosis in cathepsin-K-deficient mice. *Proceedings of the National Academy of Sciences of the United States of America* **1998**, *95*, 13453-13458.

[124] Gowen, M.; Lazner, F.; Dodds, R.; Kapadia, R.; Feild, J.; Tavaria, M.; Bertoncello, I.; Drake, F.; Zavarselk, S.; Tellis, I.; Hertzog, P.; Debouck, C.; Kola, I. Cathepsin K knockout mice develop osteopetrosis due to a deficit in matrix degradation but not demineralization. *Journal of Bone and Mineral Research* **1999**, *14*, 1654-1663.

[125] James, I. E.; Marquis, R. W.; Blake, S. M.; Hwang, S. M.; Gress, C. J.; Ru, Y.; Zembryki, D.; Yamashita, D. S.; McQueney, M. S.; Tomaszek, T. A.; Oh, H.-J.; Gowen, M.; Veber, D. F.; Lark, M. W. Potent and selective cathepsin L inhibitors do not inhibit human osteoclast resorption *in vitro*. *Journal of Biological Chemistry* **2001**, *276*, 11507-11511.

[126] Inui, T.; Ishibashi, O.; Inaoka, T.; Origane, Y.; Kumegawa, M.; Kokubo, T.; Yamamura, T. Cathepsin K antisense oligodeoxynucleotide inhibits osteoclastic bone resorption. *Journal of Biological Chemistry* **1997**, *272*, 8109-8112.

[127] Li, Z.; Yasuda, Y.; Li, W.; Bogyo, M.; Katz, N.; Gordon, R. E.; Fields, G. B.; Broemme, D. Regulation of Collagenase Activities of Human Cathepsins by Glycosaminoglycans. *Journal of Biological Chemistry* **2004**, *279*, 5470-5479.

[128] Kiviranta, R.; Morko, J.; Uusitalo, H.; Aro, H. T.; Vuorio, E.; Rantakokko, J. Accelerated turnover of metaphyseal trabecular bone in mice overexpressing cathepsin K. *Journal of Bone and Mineral Research* **2001**, *16*, 1444-1452.

[129] Bromme, D.; Klaus, J. L.; Okamoto, K.; Rasnick, D.; Palmer, J. T. Peptidyl vinyl sulphones: a new class of potent and selective cysteine protease inhibitors: S2P2 specificity of human cathepsin O2 in comparison with cathepsins S and L. *Biochemical Journal* **1996**, *315*, 85-89.

[130] Xia, L.; Kilb, J.; Wex, H.; Li, Z.; Lipyansky, A.; Breuil, V.; Stein, L.; Palmer, J. T.; Dempster, D. W.; Bromme, D. Localization of rat cathepsin K in osteoclasts and resorption pits. Inhibition of bone resorption and cathepsin K-activity by peptidyl vinyl sulfones. *Biological Chemistry* **1999**, *380*, 679-687.

[131] Punturieri, A.; Filippov, S.; Allen, E.; Caras, I.; Murray, R.; Reddy, V.; Weiss, S. J. Regulation of elastinolytic cysteine proteinase activity in normal and cathepsin K-deficient human macrophages. *Journal of Experimental Medicine* **2000**, *192*, 789-799.

[132] Chiellini, C.; Costa, M.; Novelli, S. E.; Amri, E.-Z.; Benzi, L.; Bertacca, A.; Cohen, P.; Del Prato, S.; Friedman, J. M.; Maffei, M. Identification of cathepsin K as a novel marker of adiposity in white adipose tissue. *Journal of Cellular Physiology* **2003**, *195*, 309-321.

[133] Tepel, C.; Bromme, D.; Herzog, V.; Brix, K. Cathepsin K in thyroid epithelial cells: Sequence, localization and possible function in extracellular proteolysis of thyroglobulin. *Journal of Cell Science* **2000**, *113*, 4487-4498.

[134] Buhling, F.; Roecken, C.; Brasch, F.; Hartig, R.; Yasuda, Y.; Saftig, P.; Broemme, D.; Welte, T. Pivotal role of cathepsin K in lung fibrosis. *American Journal of Pathology* **2004**, *164*, 2203-2216.

[135] Oksjoki, S.; Soderstrom, M.; Vuorio, E.; Anttila, L. Differential expression patterns of cathepsins B, H, K, L and S in the mouse ovary. *Molecular Human Reproduction* **2001**, *7*, 27-34.

[136] Kannangai, R.; Diehl, A. M.; Sicklick, J.; Rojkind, M.; Thomas, D.; Torbenson, M. Hepatic angiomyolipoma and hepatic stellate cells share a similar gene expression profile. *Human Pathology* **2005**, *36*, 341-347.

[137] Anway, M. D.; Wright, W. W.; Zirkin, B. R.; Korah, N.; Mort, J. S.; Hermo, L. Expression and localization of cathepsin K in adult rat Sertoli cells. *Biology of Reproduction* **2004**, *70*, 562-569.

[138] Buehling, F.; Peitz, U.; Krueger, S.; Kuester, D.; Vieth, M.; Gebert, I.; Roessner, A.; Weber, E.; Malfertheiner, P.; Wex, T. Cathepsins K, L, B, X and W are differentially expressed in normal and

chronically inflamed gastric mucosa. *Biological Chemistry* **2004**, *385*, 439-445.

[139] Hummel, K. M.; Petrow, P. K.; Franz, J. K.; Muller-Ladner, U.; Aicher, W. K.; Gay, R. E.; Bromme, D.; Gay, S. Cysteine proteinase cathepsin K mRNA is expressed in synovium of patients with rheumatoid arthritis and is detected at sites of synovial bone destruction. *Journal of Rheumatology* **1998**, *25*, 1887-1894.

[140] Seemayer, C. A.; Kuchen, S.; Kuenzler, P.; Rihoskova, V.; Rethage, J.; Aicher, W. K.; Michel, B. A.; Gay, R. E.; Kyburz, D.; Neidhart, M.; Gay, S. Cartilage destruction mediated by synovial fibroblasts does not depend on proliferation in rheumatoid arthritis. *American Journal of Pathology* **2003**, *162*, 1549-1557.

[141] Brubaker, K. D.; Vessella, R. L.; True, L. D.; Thomas, R.; Corey, E. Cathepsin K mRNA and protein expression in prostate cancer progression. *Journal of Bone and Mineral Research* **2003**, *18*, 222-230.

[142] Buhling, F.; Waldburg, N.; Gerber, A.; Hackel, C.; Kruger, S.; Reinhold, D.; Bromme, D.; Weber, E.; Ansorge, S.; Welte, T. Cathepsin K expression in human lung. *Advances in Experimental Medicine and Biology* **2000**, *477*, 281-286.

[143] Liu, J.; Sukhova, G. K.; Sun, J.-S.; Xu, W.-H.; Libby, P.; Shi, G.-P. Lysosomal Cysteine Proteases in Atherosclerosis. *Arteriosclerosis, Thrombosis, and Vascular Biology* **2004**, *24*, 1359-1366.

[144] Morko, J. P.; Soederstroem, M.; Saeaemaenen, A. M. K.; Salminen, H. J.; Vuorio, E. I. Up regulation of cathepsin K expression in articular chondrocytes in a transgenic mouse model for osteoarthritis. *Annals of the Rheumatic Diseases* **2004**, *63*, 649-655.

[145] Hou, W.-S.; Li, Z.; Gordon, R. E.; Chan, K.; Klein, M. J.; Levy, R.; Keysser, M.; Keyszer, G.; Bromme, D. Cathepsin K is a critical protease in synovial fibroblast-mediated collagen degradation. *American Journal of Pathology* **2001**, *159*, 2167-2177.

[146] Hou, W.-S.; Li, W.; Keyszer, G.; Weber, E.; Levy, R.; Klein, M. J.; Gravallese, E. M.; Goldring, S. R.; Bromme, D. Comparison of cathepsins K and S expression within the rheumatoid and osteoarthritic synovium. *Arthritis and Rheumatism* **2002**, *46*, 663-674.

[147] Hou, W.-S.; Li, Z.; Buettner, F. H.; Bartnik, E.; Broemme, D. Cleavage site specificity of cathepsin K toward cartilage proteoglycans and protease complex formation. *Biological Chemistry* **2003**, *384*, 891-897.

[148] Delaisse, J. M.; Boyde, A.; Maconnachie, E.; Ali, N. N.; Sear, C. H. J.; Eeckhout, Y.; Vaes, G.; Jones, S. J. The effects of inhibitors of cysteine-proteinases and collagenase on the resorptive activity of isolated osteoclasts. *Bone* **1987**, *8*, 305-313.

[149] Everts, V.; Beertsen, W.; Schroeder, R. Effects of the proteinase inhibitors leupeptin and E-64 on osteoclastic bone resorption. *Calcified Tissue International* **1988**, *43*, 172-178.

[150] Marquis, R. W.; Ru, Y.; LoCastro, S. M.; Zeng, J.; Yamashita, D. S.; Oh, H.-J.; Erhard, K. F.; Davis, L. D.; Tomaszek, T. A.; Tew, D.; Salyers, K.; Proksch, J.; Ward, K.; Smith, B.; Levy, M.; Cummings, M. D.; Haltiwanger, R. C.; Trescher, G.; Wang, B.; Hemling, M. E.; Quinn, C. J.; Cheng, H. Y.; Lin, F.; Smith, W. W.; Janson, C. A.; Zhao, B.; McQueney, M. S.; D'Alessio, K.; Lee, C.-P.; Marzulli, A.; Dodds, R. A.; Blake, S.; Hwang, S.-M.; James, I. E.; Gress, C. J.; Bradley, B. R.; Lark, M. W.; Gowen, M.; Veber, D. F. Azepanone-Based Inhibitors of Human and Rat Cathepsin K. *Journal of Medicinal Chemistry* **2001**, *44*, 1380-1395.

[151] Stroup, G. B.; Lark, M. W.; Veber, D. F.; Bhattacharyya, A.; Blake, S.; Dare, L. C.; Erhard, K. F.; Hoffman, S. J.; James, I. E.; Marquis, R. W.; Ru, Y.; Vasko-Moser, J. A.; Smith, B. R.; Tomaszek, T.; Gowen, M. Potent and selective inhibition of human cathepsin K leads to inhibition of bone resorption *in vivo* in a nonhuman primate. *Journal of Bone and Mineral Research* **2001**, *16*, 1739-1746.

[152] Tavares, F. X.; Boncek, V.; Deaton, D. N.; Hassell, A. M.; Long, S. T.; Miller, A. B.; Payne, A. A.; Miller, L. R.; Shewchuk, L. M.; Wells-Knecht, K.; Willard, D. H., Jr.; Wright, L. L.; Zhou, H.-Q. Design of Potent, Selective, and Orally Bioavailable Inhibitors of Cysteine Protease Cathepsin K. *Journal of Medicinal Chemistry* **2004**, *47*, 588-599.

[153] Barrett, D. G.; Boncek, V. M.; Catalano, J. G.; Deaton, D. N.; Hassell, A. M.; Jurgensen, C. H.; Long, S. T.; McFadyen, R. B.; Miller, A. B.; Miller, L. R.; Payne, J. A.; Ray, J. A.; Samano, V.; Shewchuk, L. M.; Tavares, F. X.; Wells-Knecht, K. J.; Willard, D. H.; Wright, L. L.; Zhou, H.-Q. Q. P2-P3 conformationally constrained ketoamide-based inhibitors of cathepsin K. *Bioorganic & Medicinal Chemistry Letters* **2005**, *15*, 3540-3546.

[154] Robichaud, J.; Oballa, R.; Prasit, P.; Falgueyret, J.-P.; Percival, M. D.; Wesolowski, G.; Rodan, S. B.; Kimmel, D.; Johnson, C.; Bryant, C.; Venkatraman, S.; Setti, E.; Mendonca, R.; Palmer, J. T. A Novel Class of Nonpeptidic Biaryl Inhibitors of Human Cathepsin K. *Journal of Medicinal Chemistry* **2003**, *46*, 3709-3727.

[155] Anonymous (2004) AAE-581, Pharmaprojects, November 12, **2004**.

[156] Anonymous (2004) 462795, Pharmaprojects, November 5, **2004**.

[157] Bromme, D.; Li, Z.; Barnes, M.; Mehler, E. Human cathepsin V functional expression, tissue distribution, electrostatic surface potential, enzymatic characterization, and chromosomal localization. *Biochemistry* **1999**, *38*, 2377-2385.

[158] Villadangos, J. A.; Bryant, R. A.; Deussing, J.; Driessen, C.; Lennon-Dumenil, A. M.; Riese, R. J.; Roth, W.; Saftig, P.; Shi, G. P.; Chapman, H. A.; Peters, C.; Ploegh, H. L. Proteases involved in MHC class II antigen presentation. *Immunological Reviews* **1999**, *172*, 109-120.

[159] Deussing, J.; Roth, W.; Saftig, P.; Peters, C.; Ploegh, H. L.; Villadangos, J. A. Cathepsins B and D are dispensable for major histocompatibility complex class II-mediated antigen presentation. *Proceedings of the National Academy of Sciences of the United States of America* **1998**, *95*, 4516-4521.

[160] Nakagawa, T. Y.; Brissette, W. H.; Lira, P. D.; Griffiths, R. J.; Petrushova, N.; Stock, J.; McNeish, J. D.; Eastman, S. E.; Howard, E. D.; Clarke, S. R. M.; Rosloniec, E. F.; Elliott, E. A.; Rudensky, A. Y. Impaired invariant chain degradation and antigen presentation and diminished collagen-induced arthritis in cathepsin S null mice. *Immunity* **1999**, *10*, 207-217.

[161] Villadangos, J. A.; Ploegh, H. L. Proteolysis in MHC class II antigen presentation: Who's in charge? *Immunity* **2000**, *12*, 233-239.

[162] Thurmond, R. L.; Sun, S.; Karlsson, L.; Edwards, J. P. Cathepsin S inhibitors as novel immunomodulators. *Current Opinion in Investigational Drugs (Thomson Scientific)* **2005**, *6*, 473-482.

[163] Urbich, C.; Heeschen, C.; Aicher, A.; Sasaki, K.-i.; Bruhl, T.; Farhadi, M. R.; Vajkoczy, P.; Hofmann, W. K.; Peters, C.; Pennacchio, L. A.; Abolmaali, N. D.; Chavakis, E.; Reinheckel, T.; Zeiher, A. M.; Dimmeler, S. Cathepsin L is required for endothelial progenitor cell-induced neovascularization. *Nature Medicine* **2005**, *11*, 206-213.

[164] Yasuda, Y.; Li, Z.; Greenbaum, D.; Bogyo, M.; Weber, E.; Broemme, D. Cathepsin V, a novel and potent elastolytic activity expressed in activated macrophages. *Journal of Biological Chemistry* **2004**, *279*, 36761-36770.

[165] McGrath, M. E.; Klaus, J. L.; Barnes, M. G.; Broemme, D. Crystal structure of human cathepsin K complexed with a potent inhibitor. *Nature Structural Biology* **1997**, *4*, 105-109.

[166] Hastings, G. A.; Adams, M. D.; Fraser, C. M.; Lee, N. H.; Kirkness, E. F.; Blake, J. A.; Fitzgerald, L. M.; Drake, F. H.; Gowan, M. Recombinant preparation of human osteoclast-derived cathepsin. *PCT Int. Appl.* WO 9524182, Sept. 14, **1995**.

[167] Li, Y. P.; Alexander, M.; Wucherpfennig, A. L.; Yelick, P.; Chen, W.; Stashenko, P. Cloning and complete coding sequence of a novel human cathepsin expressed in giant cells of osteoclastomas. *Journal of Bone and Mineral Research* **1995**, *10*, 1197-1202.

[168] Shi, G. P.; Chapman, H. A.; Bhairi, S. M.; DeLeeuw, C.; Reddy, V. Y.; Weiss, S. J. Molecular cloning of human cathepsin O, a novel endoproteinase and homologue of rabbit OC2. *FEBS Lett.* **1995**, *357*, 129-134.

[169] Catalano, J. G.; Deaton, D. N.; Furfine, E. S.; Hassell, A. M.; McFadyen, R. B.; Miller, A. B.; Miller, L. R.; Shewchuk, L. M.; Willard, D. H.; Wright, L. L. Exploration of the P1 SAR of aldehyde cathepsin K inhibitors. *Bioorganic & Medicinal Chemistry Letters* **2004**, *14*, 275-278.

[170] Boros, E. E.; Deaton, D. N.; Hassell, A. M.; McFadyen, R. B.; Miller, A. B.; Miller, L. R.; Paulick, M. G.; Shewchuk, L. M.; Thompson, J. B.; Willard, D. H.; Wright, L. L. Exploration of the P2-P3 SAR of aldehyde cathepsin K inhibitors. *Bioorganic & Medicinal Chemistry Letters* **2004**, *14*, 3425-3429.

[171] Deaton, D. N.; McFadyen, R. B.; Tavares, F. X.; Thompson, J. B.; Wright, L. L., unpublished results.

[172] Zhao, B.; Janson, C. A.; Amegadzie, B. Y.; D'Alessio, K.; Griffin, C.; Hanning, C. R.; Jones, C.; Kurdyla, J.; McQueney, M.; Qiu, X.; Smith, W. W.; Abdel-Meguid, S. S. Crystal structure of human

osteoclast cathepsin K complex with E-64. *Nature Structural Biology* **1997**, *4*, 109-111.

[173] Galpin, I. J.; Wilby, A. H.; Place, G. A.; Beynon, R. J. Synthetic analogs of the proteinase inhibitor: chymostatin. *International Journal of Peptide & Protein Research* **1984**, *23*, 477-486.

[174] Adkison, K. K.; Barrett, D. G.; Deaton, D. N.; Gampe, R. T.; Hassell, A. M.; Long, S. T.; McFadyen, R. B.; Miller, A. B.; Miller, L. R.; Payne, J. A.; Shewchuk, L. M.; Wells-Knecht, K. J.; Willard, D. H.; Wright, L. L. Semicarbazone-based inhibitors of cathepsin K, are they prodrugs for aldehyde inhibitors? *Bioorganic & Medicinal Chemistry Letters* **2005**, *15*, accepted for publication.

[175] Deaton, D. N.; Wadman, S. N.; Wright, L. L., unpublished results.

[176] Carr, T. J.; Desjarlais, R. L.; Gallagher, T. F.; Halbert, S. M.; Oh, H.-J.; Thompson, S. K.; Veber, D. F.; Yamashita, D. S.; Yen, J. H. Preparation of hydrazidyl, bis-hydrazidyl, and bis-aminomethyl carbonyl protease inhibitors. *PCT Int. Appl.* WO 9716433, May 9, **1997**.

[177] Feldman, P. L.; Brackeen, M. F.; Cowan, D. J.; Marron, B. E.; Schoenen, F. J.; Stafford, J. A.; Suh, E. M.; Domanico, P. L.; Rose, D.; Leesnitzer, M. A.; Brawley, E. S.; Strickland, A. B.; Verghese, M. W.; Connolly, K. M.; Bateman-Fite, R.; Noel, L. S.; Sekut, L.; Stimpson, S. A. Phosphodiesterase Type IV Inhibition. Structure-Activity Relationships of 1,3-Disubstituted Pyrrolidines. *Journal of Medicinal Chemistry* **1995**, *38*, 1505-1510.

[178] Deaton, D. N.; Hassell, A. M.; McFadyen, R. B.; Miller, A. B.; Miller, L. R.; Shewchuk, L. M.; Tavares, F. X.; Willard, D. H.; Wright, L. L. Novel and potent cyclic cyanamide-based cathepsin K inhibitors. *Bioorganic & Medicinal Chemistry Letters* **2005**, *15*, 1815-1819.

[179] Barrett, D. G.; Deaton, D. N.; Hassell, A. M.; McFadyen, R. B.; Miller, A. B.; Miller, L. R.; Payne, J. A.; Shewchuk, L. M.; Willard, D. H., Jr.; Wright, L. L. Acyclic cyanamide-based inhibitors of cathepsin K. *Bioorganic & Medicinal Chemistry Letters* **2005**, *15*, 3039-3043.

[180] Barrett, D. G.; Clay, W.C.; Deaton, D.N.; Hassell, A.M.; Hoffman, C.R.; Jurgensen, C.H.; Long, S.T.; McFadyen, R.B.; Miller, A.B.; Miller, L.R.; Payne, J.A.; Shewchuk, L.M.; Tavares, F.X.; Wells-Knecht, K.J.; Willard, D.H. Jr.; Wright, L.L. In *3rd International Conference on Cysteine Proteinases and their Inhibitors*; Dolinar, M., Turk, B., and Turk, V., Ed.; Garamond d. o. o., Ljubljana, Slovenia: Portoroz, Slovenia, 2002, p 95.

[181] Tavares, F. X.; Deaton, D. N.; Miller, A. B.; Miller, L. R.; Wright, L. L. Ketoheterocycle-based inhibitors of cathepsin K: A novel entry into the synthesis of peptidic ketoheterocycles. *Bioorganic & Medicinal Chemistry Letters* **2005**, *15*, 3891-3895.

[182] Catalano, J. G.; Deaton, D. N.; Long, S. T.; McFadyen, R. B.; Miller, L. R.; Payne, J. A.; Wells-Knecht, K. J.; Wright, L. L. Design of small molecule ketoamide-based inhibitors of cathepsin K. *Bioorganic & Medicinal Chemistry Letters* **2004**, *14*, 719-722.

[183] Barrett, D. G.; Catalano, J. G.; Deaton, D. N.; Long, S. T.; Miller, L. R.; Tavares, F. X.; Wells-Knecht, K. J.; Wright, L. L.; Zhou, H.-Q. Q. Orally bioavailable small molecule ketoamide-based inhibitors of cathepsin K. *Bioorganic & Medicinal Chemistry Letters* **2004**, *14*, 2543-2546.

[184] Barrett, D. G.; Catalano, J. G.; Deaton, D. N.; Long, S. T.; McFadyen, R. B.; Miller, A. B.; Miller, L. R.; Wells-Knecht, K. J.; Wright, L. L. A structural screening approach to ketoamide-based inhibitors of cathepsin K. *Bioorganic & Medicinal Chemistry Letters* **2005**, *15*, 2209-2213.

[185] Barrett, D. G.; Catalano, J. G.; Deaton, D. N.; Hassell, A. M.; Long, S. T.; Miller, A. B.; Miller, L. R.; Ray, J. A.; Samano, V.; Shewchuk, L. M.; Wells-Knecht, K. J.; Willard, D. H.; Wright, L. L. Novel, potent P^2-P^3 pyrrolidine derivatives of ketoamide-based cathepsin K inhibitors. *Bioorganic & Medicinal Chemistry Letters* **2005**, submitted for publication.

[186] Deaton, D. N.; Barrett, D. G.; Catalano, J. G.; Hassell, A. M.; Long, S. T.; Miller, A. B.; Miller, L. R.; Ray, J. A.; Samano, V.; Shewchuk, L. M.; Wells-Knecht, K. J.; Willard, D. H.; Wright, L. L. In *4th General Meeting of the International Proteolysis Society* Quebec City, Canada, **2005**.

[187] Barrett, D. G.; Catalano, J. G.; Deaton, D. N.; Hassell, A. M.; Long, S. T.; Miller, A. B.; Miller, L. R.; Shewchuk, L. M.; Wells-Knecht, K. J.; Willard, D. H., Jr.; Wright, L. L. Potent and selective P2-P3 ketoamide inhibitors of cathepsin K with good pharmacokinetic properties *via* favorable P1', P1, and/or P3 substitutions. *Bioorganic & Medicinal Chemistry Letters* **2004**, *14*, 4897-4902.

[188] Tavares, F. X.; Deaton, D. N.; Miller, A. B.; Miller, L. R.; Wright, L. L.; Zhou, H.-Q. Potent and Selective Ketoamide-Based Inhibitors of Cysteine Protease, Cathepsin K. *Journal of Medicinal Chemistry* **2004**, *47*, 5049-5056.

[189] Tavares, F. X.; Deaton, D. N.; Miller, L. R.; Wright, L. L. Ketoamide-Based Inhibitors of Cysteine Protease, Cathepsin K: P3 Modifications. *Journal of Medicinal Chemistry* **2004**, *47*, 5057-5068.

[190] Barrett, D. G., Boncek, V., Catalano, J. G., Clay, W.C., Deaton, D.N., Hassell, A.M., Hoffman, C.R., Jurgensen, C.H., Long, S.T., McFadyen, R.B., Miller, A.B., Miller, L.R., Payne, J.A., Ray, J. A., Samano, V., Shewchuk, L.M., Tavares, F.X., Wells-Knecht, K.J., Willard, D.H. Jr., Wright, L.L., Zhou, H.-Q. Q. In *4th International Conference on Cysteine Proteinases and their Inhibitors*; Dolinar, M., Turk, B., Eds.; Garamond d. o. o., Ljubljana, Slovenia: Portoroz, Slovenia, **2004**, p 83.

[191] Deaton, D. N.; Miller, L. R.; Payne, J. A., unpublished results.

[192] Hahn, T. J.; Westbrook, S. L.; Halstead, L. R. Cortisol modulation of osteoblast metabolic activity in cultured neonatal rat bone. *Endocrinology* **1984**, *114*, 1864-1870.

[193] Conaway, H. H.; Grigorie, D.; Lerner, U. H. Differential effects of glucocorticoids on bone resorption in neonatal mouse calvariae stimulated by peptide and steroid-like hormones. *J. Endocrinol.* **1997**, *155*, 513-521.

[194] Nicholson, G. C.; Malakellis, M.; Collier, F. M.; Cameron, P. U.; Holloway, W. R.; Gough, T. J.; Gregorio-King, C.; Kirkland, M. A.; Myers, D. E. Induction of osteoclasts from CD14-positive human peripheral blood mononuclear cells by receptor activator of nuclear factor kB ligand (RANKL). *Clinical Science* **2000**, *99*, 133-140.

[195] Borthakur, A.; Shapiro, E. M.; Beers, J.; Kudchodkar, S.; Kneeland, J. B.; Reddy, R. Effect of IL-1beta-induced macromolecular depletion on residual quadrupolar interaction in articular cartilage. *J. Magn. Reson. Imaging* **2002**, *15*, 315-323.

[196] Conway, J. G.; Deaton, D. N.; Miller, L. R., unpublished results.

[197] Thompson, D. D.; Seedor, J. G.; Fisher, J. E.; Rosenblatt, M.; Rodan, G. A. Direct action of the parathyroid hormone-like human hypercalcemic factor on bone. *Proceedings of the National Academy of Sciences of the United States of America* **1988**, *85*, 5673-5677.

[198] Kiviranta, R.; Morko, J.; Alatalo, S. L.; NicAmhlaoibh, R.; Risteli, J.; Laitala-Leinonen, T.; Vuorio, E. Impaired bone resorption in cathepsin K-deficient mice is partially compensated for by enhanced osteoclastogenesis and increased expression of other proteases *via* an increased RANKL/OPG ratio. *Bone* **2005**, *36*, 159-172.

[199] Anonymous (2004) Cathepsin K inhibitors, Merck & Co/Celera, R & D Focus, August 2, **2004**.